Anhydrous Partial Melting Experiments on MORB-like Eclogite: Phase Relations, Phase Compositions and Mineral–Melt Partitioning of Major Elements at 2–3 GPa

MAIK PERTERMANN[1,2]* AND MARC M. HIRSCHMANN[2]

[1]EIDGENÖSSISCHE TECHNISCHE HOCHSCHULE, INSTITUT FÜR MINERALOGIE UND PETROGRAPHIE, ETH-ZENTRUM, CH-8092 ZÜRICH, SWITZERLAND

[2]DEPARTMENT OF GEOLOGY AND GEOPHYSICS, UNIVERSITY OF MINNESOTA, 310 PILLSBURY DRIVE SE, MINNEAPOLIS, MN 55455, USA

RECEIVED NOVEMBER 18, 2002; ACCEPTED JUNE 6, 2003

We present melt and mineral compositions from nominally anhydrous partial melting experiments at 2–3 GPa on a quartz eclogite composition (G2) similar to average oceanic crust. Near-solidus partial melts at 3 GPa, determined with melt traps of vitreous carbon spheres, have 55–57 wt % SiO_2, rather less silica than the dacitic compositions that are generally assumed for near-solidus eclogite partial melts. At 2 GPa, equivalent near-solidus partial melts are less silicic (≤52 wt % SiO_2). The 3 GPa near-solidus partial melts (up to melt fractions of ~3%) are saturated in rutile and have 5·7–6·7 wt % TiO_2. The G2 composition is K_2O-poor (0·03 wt %), but a modified composition with 0·26 wt % K_2O (G2K) produces dacitic near-solidus melts with 61–64 wt % SiO_2. Rutile saturation for G2K extends to higher melt fraction (~13%) and occurs at lower TiO_2 melt contents (3·3 wt %) than for G2. These results can be understood in terms of a simplified thermodynamic model in which alkalis increase the SiO_2 content of liquids saturated in quartz, which in turn diminishes the TiO_2 concentrations required to maintain rutile saturation. Additionally, the mode of residual garnet and generation of silicic liquids by partial melting of anhydrous eclogite are linked, as garnet is required to mass-balance formation of appreciable SiO_2-rich melt. Partitioning of Na between clinopyroxene and melt shows significant increases with pressure, but only modest shifts with changing temperature. In contrast, partitioning of Ti between cpx and melt, as well as between cpx and garnet, shows pronounced dependence on temperature for compositions relevant to anhydrous partial melting of eclogite. Mixtures between partial melts of eclogite and primitive picritic Hawaiian magmas are similar to magnesian, SiO_2-rich compositions inferred from melt inclusions from the Koolau volcano. However, in detail, no eclogitic partial melt has been identified that is capable of explaining all of the compositional features of the exotic Koolau component. Based on phase compositions in our experiments, the calculated density of near-solidus eclogite is 3440 kg/m^3, notably less than commonly assumed. Therefore, the excess temperature required for a plume to support a given proportion of eclogite in the upper mantle may be less than previously assumed.

KEY WORDS: *eclogite; experimental petrology; mantle melting; partial melt; pyroxenite*

INTRODUCTION

It is well recognized that partial melting of peridotite in the upper mantle is the primary source of basaltic magmatism on Earth (e.g. Basaltic Volcanism Study Project, 1981). However, trace element and isotopic evidence demonstrates that the upper mantle is heterogeneous, and it is widely believed that observed variations in isotope and trace element compositions of basalt source regions are associated with major element or lithologic heterogeneities (e.g. Zindler *et al.*, 1984; Zindler & Hart, 1986; Weaver, 1991). Consequently, it

*Corresponding author. Telephone: +41 1 632 75 92. Fax: +41 1 632 10 88. E-mail: maik.pertermann@erdw.ethz.ch

Journal of Petrology 44(12)

is important to understand the partial melting relations of plausible non-peridotitic lithologies in basalt source regions.

Evidence from peridotite massifs (Kornprobst, 1969; Dickey, 1970; Nicolas *et al*., 1972; Loubet & Allègre, 1982) suggests that some lithologic heterogeneities in the mantle are broadly basaltic in composition. One likely origin for these lithologies is from recycling of ancient subducted oceanic crust, although other origins are also plausible [see Hirschmann & Stolper (1996) for a summary]. Eclogite xenoliths from a number of localities have been interpreted as remnants of Archaean oceanic crust (Jacob *et al*., 1994; Schulze *et al*., 2000; Barth *et al*., 2001), which implies that subduction began early in Earth history. Over time, a volume amounting to ~15–20% of the total silicate Earth is likely to have been recycled into the mantle (Chase & Patchett, 1988; Hofmann, 1997). Roughly a quarter of this subducted crust at present may reside near the core–mantle boundary (Hofmann, 1997; Rudnick *et al*., 2000). A significant fraction of it may have been destroyed by convecting, stretching and diffusion (e.g. Kellogg & Turcotte, 1990), although most recent evaluations suggest that this is a relatively inefficient process (van Keken *et al*., 2002). Much of the destruction may take place during partial melting beneath ridges (Morgan & Morgan, 1999; Helffrich & Wood, 2001).

Contributions from a basaltic pyroxenite or eclogite in the source may explain some geochemical characteristics of mid-ocean ridge basalt (MORB; e.g. Lundstrom *et al*., 1995; Hirschmann & Stolper, 1996; Niu & Batiza 1997; Eiler *et al*., 2000). Similarly, isotope and trace element systematics in ocean island basalts (OIB) may require a significant component of recycled oceanic crust (Chase, 1981; Hofmann & White, 1982; Weaver, 1991), although they may not require that the signature of recycled crust enters into modern basalt regions in non-peridotitic hosts (e.g. Putirka, 1999). Indeed, the possibility of a pyroxenite component in the sources of oceanic basalts remains controversial (Stracke *et al*., 1999; Becker, 2000).

A relatively recent development is that some enriched isotopic components in oceanic basalts have been tied to distinct major element characteristics and these correlations have been attributed to partial melts of non-peridotitic lithologies in basalt source regions. Hauri (1996) and Lassiter & Hauri (1998) identified the Koolau volcanic trend of Hawaii as having a unique major element composition that correlates with elevated $^{187}Os/^{188}Os$ and other isotopic traits indicative of an enriched component. The salient major element feature of this component is enrichment in silica, which Hauri (1996) attributed to a dacitic partial melt of recycled oceanic crust. Takahashi & Nakajima (2002) also argued for a recycled eclogitic source for this component, although they considered the partial melt composition to be that of basaltic andesite, rather than dacite. On the other hand, the presence of mafic heterogeneities in the Hawaiian source has been challenged based on isotopic evidence (e.g. Stracke *et al*., 1999).

Among OIB, the HIMU-basalts (high $^{238}U/^{204}Pb$) are considered to have the strongest isotopic signature of recycled oceanic crust (e.g. Hofmann, 1997). It is therefore notable that lavas with extreme HIMU signatures have major element compositions distinct from non-HIMU OIB lavas: they are slightly depleted in SiO_2, K_2O and P_2O_5, and more enriched in CaO, FeO* and MnO (Kogiso *et al*.,1997*a*). It should be noted that these characteristics are very different from the putative silicic Koolau component (Hauri, 1996). Although the origin of the HIMU major element component is not known, several scenarios involving pyroxene-rich lithologies such as peridotite–basalt mixtures (Kogiso *et al*., 1998) and garnet pyroxenite (Hirschmann *et al*., 2003) have been investigated.

Recycled basaltic pyroxenite may also play an important role in the source regions of large igneous provinces (LIPs). In particular, several workers have suggested that relatively easily fused pyroxenite may be responsible for high melt production rates required to feed flood basalt provinces (Cordery *et al*., 1997; Takahashi *et al*., 1998; Yasuda & Fujii, 1998; Leitch & Davies, 2001). For example, Takahashi *et al*. (1998) proposed melting of a heterogeneous plume head to explain rapid production of large volumes of lavas in the Columbia River Basalts (CRB) of the NW USA. In their model, pyroxenite lithologies entrained in the plume head begin to melt below the solidus of the surrounding peridotite. This melt pools at the top of the pyroxenite heterogeneities and then reaches the surface in the form of large basaltic lava flows. Formation of basaltic magmas from pyroxenite requires a high degree of melting, as has been shown by experiments on the most primitive CRB lavas (Takahashi *et al*., 1998). Also, the partial melts must not have appreciable garnet in their source, as erupted CRB lack strong depletions of heavy rare earth elements (HREE) relative to light REE (LREE; Wright *et al*., 1988).

Despite the apparent significance of basaltic pyroxenite or eclogite in basalt formation, relatively little is known about their partial melting behavior under volatile-poor conditions. Most experimental studies date back to the 1970s [see Hirschmann & Stolper (1996) and references therein] and provide little detailed information about phase compositions and proportions. Many also have well-known problems with Fe loss to sample containers and with volatile

Table 1: Composition of starting materials in selected eclogite partial melting studies

	This study		Other studies			
	G2	G2K	CRB72-31	GA1	CLG46	SBM6
SiO_2	50·05(23)	50·81(15)	50·76	50·35	40·77	52·0
TiO_2	1·97(9)	1·90(6)	1·48	1·49	1·11	4·5
Al_2O_3	15·76(24)	15·22(8)	16·02	16·53	15·15	18·5
FeO*	9·35(19)	9·03(12)	9·52	9·83	12·55	—
MnO	0·19(3)	0·16(3)	0·14	0·17	0·22	—
MgO	7·90(12)	7·91(7)	8·23	7·94	8·07	8·8
CaO	11·74(20)	11·68(9)	10·77	9·6	9·59	11·0
Na_2O	3·04(10)	3·02(7)	2·29	3·49	2·74	4·0
K_2O	0·03(3)	0·26(2)	0·39	0·44	0·01	1·2
P_2O_5	—	—	0·14	0·16	—	—
Sum	100·00	100·00	99·60	99·84	99·90	100·0
Mg no.	60·1	61·0	60·6	59·0	54·0	

FeO*, all Fe reported as FeO. CRB72-31 is the starting material of Takahashi *et al*. (1998); GA1 is from Yaxley & Green (1998); CLG46 is the model Archaean composition of Takahashi & Nakajima (2002); SBM6 is the Fe-free synthetic starting material of Klemme *et al*. (2002). G2 and G2K totals were normalized to 100 wt %, all other data are given as originally reported.

contamination. Several more recent studies on natural compositions exist, most notably those by Johnston (1986), Yasuda *et al*. (1994), Yaxley & Green (1998) and Takahashi & Nakajima (2002), but no previous work reports detailed phase proportions and compositions through the melting interval of a basaltic pyroxenite.

In this paper we report the glass and mineral compositions from a series of partial melting experiments on a basaltic eclogite composition (G2, Table 1) at 2–3 GPa. These experiments also form the basis for a companion paper (Pertermann & Hirschmann, 2003), in which we discuss solidus location, melt production and proportions of phases in the melting interval, with an emphasis on the likely effects of such compositions on melt production and on trace element characteristics of MORB. Here we focus on the major element compositions of the partial melts and on petrologic aspects of the mineral and melt compositions.

EXPERIMENTAL AND ANALYTICAL PROCEDURES

Experimental procedures have been described in part by Pertermann & Hirschmann (2003). Here we briefly describe key points and add explanatory material not included in the companion paper. The starting material, G2 (Table 1), is derived from natural garnet and clinopyroxene [both from Bavarian eclogite W6.8 (Stosch & Lugmair, 1990)], natural quartz and kyanite, and synthetic TiO_2. The composition was chosen to be similar to present-day mid-oceanic crust in terms of most major elements (Pertermann & Hirschmann, 2003). Partial melting experiments were conducted with a $\frac{1}{2}$ inch (12·7 mm) end-loaded piston cylinder apparatus, using pressure cells consisting of $BaCO_3$ sleeves, straight graphite heaters, and internal spacers of crushable MgO. All experiments were conducted using the hot piston-in technique with a pressure correction of −0·2 GPa. Runs were pressurized cold to 0·5 GPa and then heated to 500°C to soften the assembly before further pressurization. Then pressure and temperature were raised simultaneously, staying well below the solidus to avoid disequilibrium melting during pressurization. The assembly was pressurized to 0·05–0·1 GPa below the desired run pressure, and the final pressure adjustment was made at run temperature. Pressure and temperature uncertainties are believed to be ±0·1 GPa and ±12°C, respectively [see Xirouchakis *et al*. (2001) for calibration details of this particular apparatus]. Power consumption was monitored throughout experiments and generally increased by ≤3% (relative) within the first hours before leveling off. The temperature was maintained to within ±1°C by an Eurotherm 818P controller, and pressure was within ±1–2% (relative) of the nominal run pressure, as monitored by a Heise gauge.

Finely powdered (<15 μm) sample was placed in thick-walled graphite capsules, which were welded inside Pt outer capsules. Stringent steps were taken to ensure near-anhydrous conditions (Pertermann &

Hirschmann, 2003). Near-solidus runs contained a layer of vitreous carbon spheres (80–150 μm diameter) to allow determination of partial melt compositions (Pickering-Witter & Johnston, 2000; Schwab & Johnston, 2001; Wasylenki *et al.*, 2003). The spheres may also absorb water potentially present in the charge (Robinson *et al.*, 1998), further assuring anhydrous conditions. The use of graphite capsules and furnaces limited the oxygen fugacity to below the graphite–CO buffer (Taylor & Green, 1989; Ulmer & Luth, 1991).

Major element analysis of experimental run products was performed by wavelength-dispersive electron microprobe analysis with the JEOL JXA8900R at the University of Minnesota. Operating conditions were an acceleration voltage of 15 kV, beam currents of 7·5–15 nA, and ZAF data reduction with software supplied by JEOL. A fully focused beam (1–2 μm diameter) of 7·5 nA was used to analyze the glass rims around vitreous carbon spheres and garnet and pyroxene grains with peak counting times of 30 s and 15 s on each side of the background (procedure A). For glasses in the higher melt fractions runs ($F > 0{\cdot}2$, procedure B), we used a 15 nA beam defocused to 15 μm diameter with 15 and 8 s counting time, respectively. The procedures yield results that are identical within error, as evidenced by similar compositions determined by analyses of secondary standard glasses.

The problem of Na loss during glass analyses was addressed in the following manner. Two basalt glasses (BHVO-2 and BCR-2 prepared by NIST from standard rocks BHVO and BCR) were analyzed with the procedure of Morgan & London (1996), using a fully focused beam at 15 kV, 2 nA and counting times of 2, 5, 10, 20 and 40 s. Ten repeat analyses for each counting time were performed; all analyses were on a new spot on the glass. The resulting Na_2O contents were extrapolated linearly to zero-time values of 2·07 ± 0·04 (BHVO-2) and 3·08 ± 0·06 wt % (BCR-2), which should closely match the true Na_2O content of the glasses. These Na_2O values for the glass samples are lower than published values for BHVO and BCR standard rocks, perhaps owing to Na_2O loss during glass preparation. The same glasses were then analyzed with our procedure B. As shown in Table 2, oxides other than Na_2O are in good agreement with the published values for BHVO and BCR, which reflects well on the overall accuracy of the analytical procedure. For Na_2O, procedure B yielded 2·04 ± 0·04 wt % for BHVO-2 and 2·93 ± 0·04 wt % for BCR-2 (Table 2). The result for BHVO-2 is in excellent agreement with the extrapolated value, and for BCR-2 it is similar within 2 SD. Consequently, glass compositions reported in this study are not corrected for Na loss.

Several precautions were taken to assure accuracy and reproducibility of analytical data, including methodical analysis of secondary standards during each analytical session, and analysis of secondary standards, such as the aforementioned BHVO-2 and BCR-2 glasses (Table 2). Additionally, standards were matched to the unknown phases and compositions: two basalt glass standards for analysis of quenched melts, natural augite and omphacite for cpx analysis, and natural pyrope-rich garnet for analysis of garnet; Ti and Mn in minerals were standardized on TiO_2-rich hornblende and Mn-hortonolite, respectively. Consistency of analyses between analytical sessions was verified via long-term monitoring of a secondary standard basalt glass (USGS 113498/1), which yielded the following relative uncertainties: SiO_2 0·5%, TiO_2 2·2%, Al_2O_3 0·9%, FeO* 1·2%, MgO 1·7%, CaO 1·4%, Na_2O 3·8%, K_2O 5·4% and MnO 19% (15 sessions, $n = 163$).

The very thin rims of glass around the vitreous carbon spheres (Fig. 1) necessitated use of a fully focused electron beam. However, the X-ray excitation volume still exceeded the thickness of the glass rims, as evidenced by analytical totals well below 100 wt %. Analytical totals less than 70 wt % were rejected and the remaining individual analyses were then normalized to 100 wt % before averaging. We note that this procedure does not include ZAF correction for the excess carbon analyzed, but linear extrapolation of oxide wt % trends as a function of analytical totals to 100 wt % yielded values in excellent agreement within error of reported analyses.

Table 2: Composition of secondary standards

	BHVO-2		BCR-2G	
	preferred	analyzed	preferred	analyzed
n		32		45
SiO_2	49·9(6)	50·1(2)	54·8(8)	54·4(3)
TiO_2	2·73(4)	2·79(4)	2·26(5)	2·32(4)
Al_2O_3	13·5(2)	13·8(7)	13·5(2)	13·7(2)
Fe_2O_3	12·3(2)	12·3(1)	13·8(2)	13·7(2)
MgO	7·23(12)	7·47(7)	3·59(5)	3·71(6)
CaO	11·4(4)	11·5(1)	7·12(11)	7·16(9)
Na_2O	2·22(8)	2·04(4)	3·16(11)	2·93(4)
K_2O	0·52(1)	0·50(2)	1·79(5)	1·75(4)
P_2O_5	0·27(2)	0·25(3)	0·35(2)	0·33(4)
Sum	100·07	100·74	99·67	100·02
Na_2O*		2·07(4)		3·08(6)

n, number of points analyzed with procedure B. All Fe analyzed as Fe_2O_3.
*Extrapolated with Morgan & London (1996) procedure.

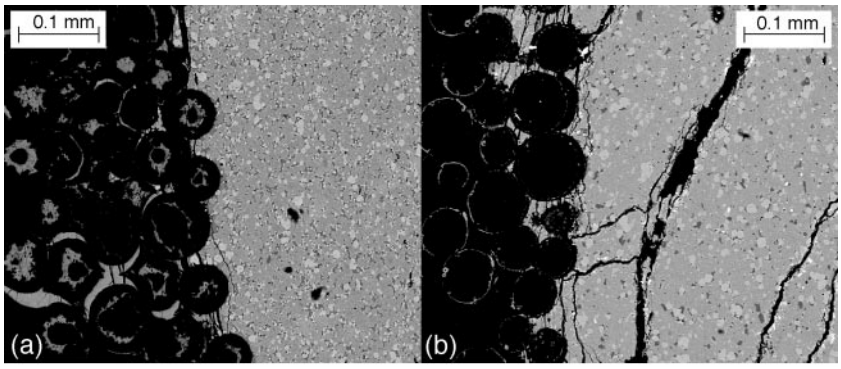

Fig. 1. Backscatter electron images of experimental charges with vitreous carbon spheres. (a) Run A188K (G2K, 1315°C, 3·0 GPa, 91·5 h); the partial melt is dacitic, resulting in relatively thick rims of glass around the vitreous carbon spheres. (b) Run A177-121 (G2, 1335°C, 3·0 GPa, 121 h); the partial melt is less silica- and alkali-rich than in (a) and observed glass rims are much thinner than in (a). The spheres in (a) [and to a lesser degree in (b)] appear to have melt inclusions, believed to be associated with the onset of devitrification of the carbon spheres. Glass composition data reported in this study are from the thin rinds, not from the inclusions in spheres. The texture shown in (b) is representative for all G2 experiments; only the G2K experiments produced thicker glass rims around the spheres.

Attainment of equilibrium

The use of vitreous carbon spheres is a variation of the diamond aggregate technique (Hirose & Kushiro, 1993; Baker & Stolper, 1994), and the latter has been subject to considerable debate about its applicability to near-solidus melting of peridotite (Baker *et al*., 1996; Falloon *et al*., 1996, 1999; Hirschmann *et al*., 1998). A thorough discussion of the advantages and disadvantages of this technique has been given by Baker & Stolper (1994), Falloon *et al*. (1999), Pickering-Witter & Johnston (2000), Schwab & Johnston (2001) and Wasylenki *et al*. (2003). We note that the vitreous carbon method differs from the diamond aggregate technique because melt is separated from the charge by surface effects (wicking), rather than owing primarily to a pressure gradient.

In runs that contained vitreous carbon, the spheres constituted 10–15% of the charge (by weight) and were present as layer 3–4 spheres deep at the bottom of the charge. The relatively short distance between glass rims and the charge suggests that diffusive equilibration should occur over ~4–10 h (Pertermann & Hirschmann, 2003). However, the time necessary to obtain completely equilibrated residual minerals is much greater. To evaluate the minimum run duration needed to produce well-equilibrated charges at feasible laboratory time scales, we conducted a series of eight experiments with variable duration (6–121 h) at 3 GPa and 1335°C.

Glass compositions were analyzed for all runs in the time series, and the resulting oxide trends are plotted in Fig. 2. After 48–72 h, the melt composition does not change significantly for any element apart from K_2O. Near the solidus, K_2O is very sensitive to melt fraction, and we attribute inconsistencies in K_2O to melt fraction variations associated with the ±12°C uncertainty in experimental conditions. For example, the run of 82 h duration (A177-82) has low K_2O and much higher melt fraction ($F = 7{\cdot}4\%$) calculated from mass balance (Table 3) than the 70, 96 and 121 h runs ($F = 2{\cdot}0$–$3{\cdot}2\%$).

With increasing run duration, grain boundaries of residual minerals are more faceted, indicating a closer approach to textural equilibrium. All runs, even after 121 h, have some zoned minerals, but we do not regard this as problematic for phase equilibria and mass balance, as the relative mass of cores is very small (Pertermann & Hirschmann, 2003). With the exception of one run at 3 GPa and 1400°C, which had a very high melt fraction, all runs that employed vitreous carbon spheres were ≥70 h to assure a close approach to equilibrium.

Owing to possible complicating effects of zoning, special care was taken during microprobe analysis of minerals. In some cases, small grain sizes (10–15 μm) made it difficult to avoid beam overlap of equilibrated rims with partially unreacted cores. Figure 3 shows analyses of a cpx that demonstrate the principle used to extract equilibrium compositions in such cases. The unequilibrated mineral cores have a different composition (higher Na_2O, lower TiO_2, etc.), caused by equilibration at a much lower temperature and probably somewhat lower pressure at eclogite-facies conditions (Stosch & Lugmair, 1990). During the course of an experiment, the mineral composition migrates away from the starting composition, and therefore we consider the far extrema of the observed range (in this case, lower Na_2O and higher TiO_2) as representative of the equilibrium mineral composition. All cpx and garnet analyses reported here are averages of analyses selected at the respective end of the oxide trends. This approach is comparable with the method

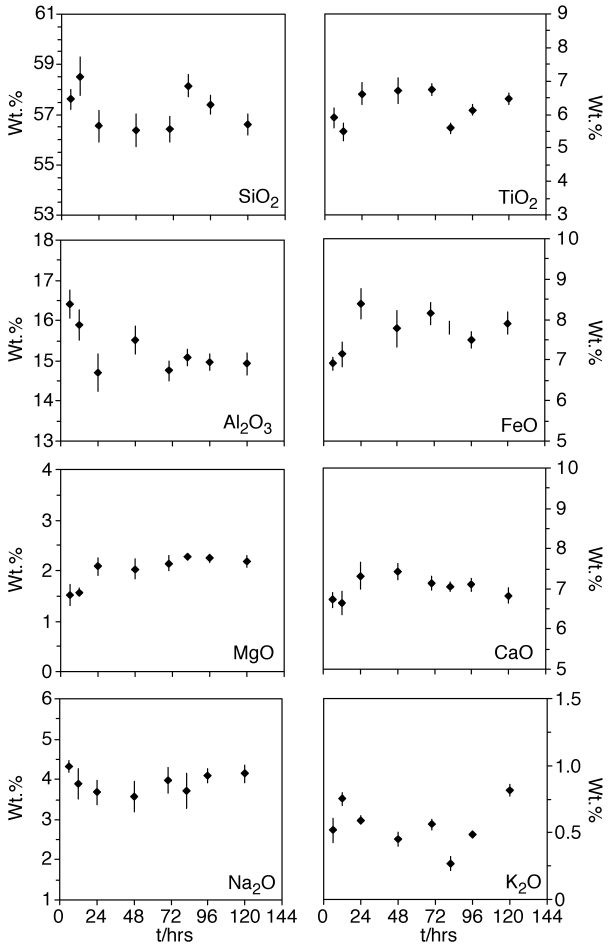

Fig. 2. Melt compositions of time-series experiments at 3·0 GPa and 1335°C, ranging in duration from 6 to 121 h. Most oxides reach steady state after 48–72 h. Melt fractions calculated from mass balance are 3·1, 7·4, 3·2 and 2·0 wt % for the runs of 70, 82, 96 and 121 h, respectively. Because K_2O is highly incompatible and therefore very sensitive to the extent of melting near the solidus, the low K_2O for the 82 h experiment also suggests an anomalously high melt fraction. We believe that the actual temperature of this run (A177-82) was higher than that of the other runs at this nominal temperature. Given the inherent ±12°C temperature uncertainty in our piston cylinder assembly and the curvature of the F vs T trend at 3 GPa (Pertermann & Hirschmann, 2003), the actual temperature may have been closer to 1350°C. All runs were saturated with quartz, but rutile was positively identified only in runs lasting 24 and 121 h. Because of the small rutile mode, this had little effect on the actual TiO_2 concentration of the partial melt and only negligible effects on residual totals in mass-balance calculations.

described by Pickering-Witter & Johnston (2000) and Schwab & Johnston (2001).

A further measure of whether equilibrium was attained in the partial melting experiments is to examine the extent to which garnet and cpx achieved Fe–Mg exchange values consistent with existing parameterizations. Here we compare the Fe–Mg exchange K_D [$= (X_{Fe}/X_{Mg})^{grt}/(X_{Fe}/X_{Mg})^{cpx}$] between garnet and cpx observed in our experiments with those calculated from the Ellis & Green (1979) and Ravna (2000) exchange thermometers.

As shown in Fig. 4, values of K_D predicted by Ravna (2000) are more similar to those observed in our experiments than are those predicted by Ellis & Green (1979), although most values predicted by both models are smaller than those observed. Also, predictions of both models agree better with observations at low temperature (larger K_D in Fig. 4) than at high temperature (smaller K_D). We also compare the predictions of both models with K_D determined from the 3·5 GPa eclogite partial melting experiments of Yaxley & Green (1998). Their experiments show good agreement with the Fe–Mg garnet–cpx exchange K_D values calculated with the model of Ellis & Green (1979) and reasonable agreement with those calculated after Ravna (2000) (Fig. 4). The more recent calibration of Ravna (2000) incorporates a larger number of experimental observations, and because it has a more complex dependence on garnet composition, one might therefore expect it to be more accurate than the Ellis & Green (1979) parameterization. However, neither model accounts for the effects of complex substitutions in cpx, which may be important for the highly aluminous cpx found in partial melting of eclogitic bulk compositions.

We note that our partial melting experiments are unreversed and were performed with natural starting materials. The Fe–Mg exchange coefficient between garnet and cpx in the W6.8 eclogite we employed (Stosch & Lugmair, 1990) is 10·1, very different from the range of values ($\sim$1·5–2·2) expected at equilibrium conditions of our experiments and from the range of values we observe (Fig. 4). We assume that mineral phases approach equilibrium over the course of the experiments, but it may be unrealistic to believe equilibration reaches completion and therefore it is not surprising that the majority of our experiments produced Fe–Mg K_D values that are slightly larger than those predicted at equilibrium. As illustrated in Fig. 4b, K_D values observed during the time series experiments at 1335°C are dramatically lower than the initial value of 10·1 and with time closely approach the equilibrium value predicted by Ravna (2000). Thus, although it is dangerous to assume *a priori* that the compositions of phases reach equilibrium in unreversed experiments, we conclude that reasonable approaches to equilibrium compositions have been achieved in the partial melting experiments presented here.

In a related study (Pertermann & Hirschmann, 2002), we investigated trace element partitioning between highly aluminous cpx and melt similar in

Table 3: Composition of glasses

Run no.:	A284	A184	A252	A202	A170	A168	A177-6	A177-12
P (GPa):	2·0	2·0	2·0	2·5	3·0	3·0	3·0	3·0
T (°C):	1250	1325	1375	1325	1315	1325	1335	1335
t (h):	82	40	15	60·5	96	92	6	12
Glass (wt %):	9·3(2·7)	48·1(1·1)	77·3(1·2)	20·2(1·3)	0(3·2)[1]	5·3(1·3)	n.d.	n.d.
Other phases:	cpx gt ru pl	cpx gt	cpx	cpx gt	cpx gt qz ru	cpx gt qz	cpx gt qz	cpx gt qz
n:	13	14	10	11	14	12	12	14
SiO_2	52·42(36)	52·55(39)	50·41(25)	58·42(64)	55·19(75)	56·35(31)	57·60(38)	58·52(76)
TiO_2	6·66(13)	2·96(11)	2·34(10)	4·23(13)	6·07(31)	6·25(15)	5·90(29)	5·48(26)
Al_2O_3	14·49(21)	17·52(15)	17·08(11)	15·51(21)	14·71(30)	14·94(19)	16·41(34)	15·90(37)
FeO*	11·41(35)	9·98(30)	9·81(15)	8·25(32)	9·06(39)	8·42(22)	6·92(16)	7·14(30)
MnO	0·12(4)	0·14(2)	0·17(4)	0·10(3)	0·10(4)	0·09(3)	0·08(3)	0·08(4)
MgO	3·25(10)	4·17(8)	6·22(10)	2·53(6)	2·22(17)	2·31(10)	1·52(21)	1·57(9)
CaO	7·74(19)	8·25(8)	10·02(13)	7·06(21)	7·84(41)	6·92(14)	6·73(19)	6·66(29)
Na_2O	3·74(35)	4·36(14)	3·41(8)	3·78(25)	3·68(38)	4·20(16)	4·33(14)	3·89(37)
K_2O	0·16(3)	0·05(1)	0·03(2)	0·13(2)	1·14(16)	0·51(4)	0·52(9)	0·75(5)
Sum	100·00	99·98(34)	99·49(33)	100·00	100·00	100·00	100·00	100·00
Mg no.	33·7	42·7	53·1	35·4	30·4	32·8	28·2	28·2

Run no.:	A177-24	A177-48	A177-70	A177-82	A177-96	A177-121	A171	A175
P (GPa):	3·0	3·0	3·0	3·0	3·0	3·0	3·0	3·0
T (°C):	1335	1335	1335	1335	1335	1335	1350	1365
t (h):	24	48	70	82	96	121	77	70·5
Glass (wt %):	n.d.	n.d.	3·1(1·3)	7·4(1·4)	3·2(1·3)	2·0(1·1)	7·9(1·2)	8·9(1·4)
Other phases:	cpx gt qz ru	cpx gt qz	cpx gt qz	cpx gt qz	cpx gt qz	cpx gt qz ru	cpx gt qz	cpx gt qz
n:	19	15	10	11	17	19	13	15
SiO_2	56·55(62)	56·38(66)	55·98(32)	57·22(51)	57·33(32)	56·62(41)	56·03(47)	56·07(18)
TiO_2	6·61(33)	6·72(39)	6·65(29)	5·66(20)	6·18(12)	6·47(18)	6·38(26)	5·89(7)
Al_2O_3	14·70(46)	15·52(35)	14·92(25)	15·35(21)	14·93(20)	14·93(27)	15·31(22)	15·37(37)
FeO*	8·38(37)	7·77(45)	8·37(24)	8·02(24)	7·54(18)	7·91(27)	8·27(31)	8·34(11)
MnO	0·09(4)	0·11(3)	0·09(4)	0·10(3)	0·09(3)	0·09(4)	0·09(4)	0·10(2)
MgO	2·08(17)	2·03(19)	2·13(13)	2·28(9)	2·24(8)	2·19(11)	2·39(10)	2·44(9)
CaO	7·32(33)	7·44(20)	7·28(25)	7·14(20)	7·12(14)	6·83(18)	7·44(22)	7·61(9)
Na_2O	3·67(31)	3·58(38)	4·02(27)	3·94(38)	4·09(19)	4·14(22)	3·77(19)	3·95(8)
K_2O	0·59(3)	0·45(5)	0·57(5)	0·28(2)	0·49(2)	0·81(4)	0·31(2)	0·24(4)
Sum	100·00	100·00	100·00	100·00	100·00	100·00	100·00	100·00
Mg no.	30·7	31·8	31·2	33·6	34·6	33·0	34·0	34·3

composition to those found at 3 GPa and 1335°C in the present work. Crystallization experiments on a synthetic mixture of oxides corresponding to the 1335°C partial melt composition under identical conditions yielded glass coexisting with cpx, garnet, quartz and rutile. This may be interpreted as a reversal, further demonstrating that the phases in the original partial melting experiments were indeed close to equilibrium.

RESULTS

Phase relations

Abundances of melt, cpx and garnet, calculated from mass balance, are listed in Tables 3–5, together with the composition data for the respective phases [see also table 2 of Pertermann and Hirschmann (2003)]. At 3 GPa, glass is present at 1315°C, but is not observed at 1300°C. Also, the run at 1300°C is texturally less mature than above-solidus charges. Sub-solidus phases

Table 3: continued

Run no.:	164	A195	A189	A190	A194	A197	A221K	A200K	A188K
P (GPa):	3·0	3·0	3·0	3·0	3·0	3·0	2·0	3·0	3·0
T (°C):	1375	1400	1425	1450	1475	1500	1325	1275	1315
t (h):	72·5	29	24	19	12	2·5	46	96	91·5
Glass (wt %):	17·9(1·2)	23·8(1·3)	36·4(1·3)	50·7(1·1)	59·8(1·4)	86·8(1·5)	51·5(8)	14·3(8)	14·5(1·1)
Other phases:	cpx gt	cpx gt	cpx gt	cpx gt	cpx gt	cpx	cpx gt	cpx gt qz ru	cpx gt qz
n:	13	13	11	12	9	13	20	13	20
SiO_2	57·00(30)	54·64(56)	53·47(24)	51·89(12)	50·91(19)	49·46(17)	52·81(20)	63·64(37)	61·49(62)
TiO_2	4·64(14)	4·54(18)	3·77(9)	3·19(4)	2·77(5)	2·02(3)	2·74(6)	3·33(8)	4·12(11)
Al_2O_3	15·69(11)	16·03(38)	15·79(10)	16·49(8)	16·33(8)	16·53(9)	17·10(9)	15·35(15)	14·52(20)
FeO*	8·46(17)	9·44(28)	9·87(10)	10·15(10)	10·02(6)	9·72(11)	9·36(10)	5·18(18)	6·20(24)
MnO	0·09(5)	0·12(2)	0·17(3)	0·15(2)	0·16(2)	0·16(3)	0·13(3)	0·06(3)	0·06(2)
MgO	2·75(16)	3·10(25)	4·00(8)	4·61(5)	5·48(5)	7·25(8)	4·02(8)	1·53(6)	1·98(7)
CaO	7·42(14)	8·22(25)	8·98(10)	9·42(8)	9·70(5)	10·93(8)	8·05(5)	4·93(15)	6·19(22)
Na_2O	3·82(12)	3·79(37)	3·35(9)	3·50(5)	3·20(7)	3·13(9)	4·21(7)	4·34(32)	4·01(17)
K_2O	0·13(1)	0·12(1)	0·07(2)	0·07(1)	0·05(1)	0·03(1)	0·52(2)	1·63(7)	1·44(6)
Sum	100·00	100·00	99·47(54)	99·45(19)	98·63(27)	99·23(32)	98·95(26)	100·00	100·00
Mg no.	36·7	37·0	54·0	44·7	49·4	57·1	43·4	34·5	36·3

Reported modes taken from Pertermann & Hirschmann (2003, table 2). Errors in parentheses for modes and compositions are one SD of the mean, reported as least units cited; 52·42(36) wt % SiO_2 should be read as 52·42 ± 0·36 wt %. n.d., glass present, but no mode calculated because of heterogeneity of residual minerals. *n*, number of points analyzed. FeO*, all Fe assumed to be FeO. Mg number is molecular Mg/(Mg + Fe) × 100.
[1]Calculated melt fraction for run A170 is zero, but glass is present in the vitrous carbon sphere aggregate (note the large error).

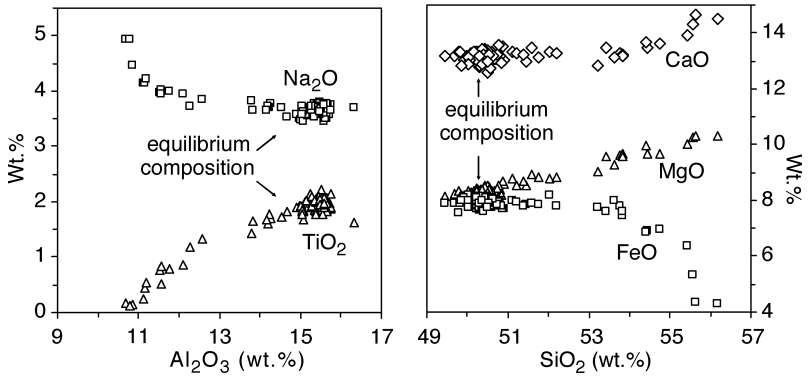

Fig. 3. This figure illustrates our technique for extracting near-equilibrium compositions from imperfectly homogenized minerals in reaction products. We analyzed a large number of grains ($n > 100$, data from run A168, 3·0 GPa and 1325°C), most of which yielded near-equilibrated compositions, but some of which were contaminated by incompletely reacted cores of eclogitic cpx starting material, which has virtually no TiO_2 and ~5 wt % Na_2O, as well as more CaO and MgO and less FeO than reacted compositions. To obtain near-equilibrium compositions, we averaged points from the cluster of data most different from the unreacted Na_2O-rich, TiO_2-poor analyses.

at 3 GPa are cpx (78%), garnet (18%), quartz (~4%), and traces of rutile. Rutile is present up to at least 1335°C, although it is not observed in all runs. Even when present, it may elude identification owing to its low modal abundance (~0·3%). Although it is observed at 1315°C, it is not found at 1325°C, and is positively identified in only two of the time series runs at 1335°C. As noted below, consistent concentrations of TiO_2 in glass, cpx and garnet in all 3 GPa runs at ≤1335°C suggest that rutile-out is located between 1335 and 1350°C. Quartz is present to 1365°C and absent at higher temperatures. At 1300–1400°C, the

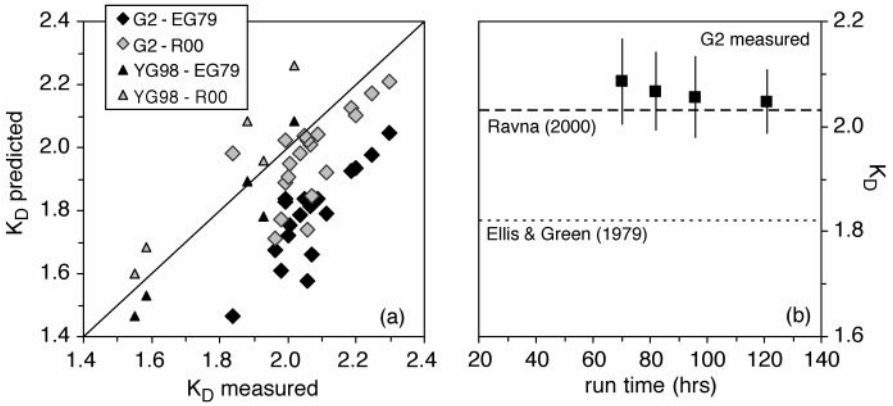

Fig. 4. (a) Fe–Mg exchange $K_D = (X_{Fe}/X_{Mg})^{grt}/(X_{Fe}/X_{Mg})^{cpx}$ between garnet and cpx measured in the G2 partial melting experiments compared with those calculated from the garnet–cpx thermometers of Ellis & Green (1979) and Ravna (2000) (EG79 and R00, respectively). Calculated K_D values use experimental temperatures, pressures, and observed Ca and Mn concentrations of garnets as inputs. Also shown are K_D values observed in the 3·5 GPa eclogite partial melting experiments of Yaxley & Green (1998) (YG98) and corresponding calculated values. (b) K_D values observed in time series experiments at 3 GPa and 1335°C compared with equilibrium K_D values calculated from Ellis & Green (1979) and Ravna (2000). The K_D between garnet and cpx in the starting composition is 10·1 (Stosch & Lugmair, 1990), and the time series demonstrates that the experimental minerals approach Fe–Mg exchange equilibrium during the duration of the experiments.

quartz to coesite transition is at 3·3–3·4 GPa (Hemingway *et al.* 1998), indicating that the silica phase in our experiments is quartz and not coesite.

The highest temperature at which garnet is observed is 1475°C. Cpx is present from below the solidus up to >1500°C. The liquidus is between 1500 and 1525°C, as only glass is observed at 1525°C. Thus the melting range for G2 spans ~200°C at 3 GPa.

The 2 GPa solidus is bracketed at 1175 ± 10°C, and sub-solidus phases are cpx, garnet, quartz, rutile and plagioclase. Quartz disappears between 1185 and 1225°C, and rutile disappears above 1250°C. Plagioclase is absent at 1325°C and above, and garnet is not observed at $T \geq 1375$°C. The estimated 2 GPa liquidus is near 1400°C, making the overall melting range slightly larger than that at 3 GPa. A single experiment at 2·5 GPa and 1325°C yielded glass, cpx and garnet.

Phase composition

In the following section, we summarize the most important compositional observations of the three principal phases, glass, clinopyroxene and garnet, as a function of pressure and temperature.

Glass

Partial melts of G2 range from andesitic near the solidus to basaltic at high melt fraction (Table 3, Fig. 5). At 3 GPa, SiO_2 increases slightly from 55·2 wt % at the solidus to ~57 wt % near the exhaustion of quartz at about 1365°C, and then decreases rapidly, reaching 49·8 wt % at 1500°C. Melts at 2 GPa are less silicic, having only 52·4 wt % SiO_2 at 1250°C and decreasing to 50·7 wt % at 1375°C. On the other hand, the glass from the sole experiment at 2·5 GPa is more silicic (58 wt %). This is unexpected, because this run has a relatively high melt fraction and lacks quartz. We have no explanation for this discrepancy, and although we report results from this run, more experiments at 2·5 GPa would be required to confirm them. Near-solidus melts at 3 GPa are also quartz normative, and become olivine normative at 1475–1500°C and $F =$ 0·60–0·87, a much higher melt fraction than observed at 2 GPa, where partial melts are quartz normative at low temperature (1250°C) and become olivine normative near 1325°C ($F \sim 0{\cdot}48$).

A key feature of the experimental glasses is their enrichment in TiO_2, particularly near the solidus. At 3 GPa the concentrations are similar: ~5·7–6·7 wt % at 1315–1335°C, conditions inferred or observed to correspond to rutile saturation. With rising temperature and increasing melt fraction, they diminish to 2 wt %, the TiO_2 content of the starting material. At 2 GPa, partial melt has 6·7 wt % TiO_2 near the solidus, which diminishes to 2·4 wt % at 1375°C.

At 3 GPa, Al_2O_3, FeO*, MgO, CaO and Mg number all increase smoothly with rising temperature and increasing melt fraction, although all show less variation below 1365°C, where quartz is saturated. Several elements, including CaO, MgO and FeO*, have kinks in their trends near 1475°C, the temperature of initial garnet saturation. Very near the solidus, FeO* and CaO depart from the trend, as the lowest melt fraction liquids are slightly enriched in FeO* and CaO, possibly reflecting other changes in melt composition under

Table 4: Composition of clinopyroxene

Run no.:	A284	A184	A252	A202	166	A170	A168	A177-70
P (GPa):	2·0	2·0	2·0	2·5	3·0	3·0	3·0	3·0
T (°C):	1250	1325	1375	1325	1300	1315	1325	1335
t (h):	82	40	15	60·5	92	96	92	70
cpx (wt %):	56·9(1·3)	48·5(1·4)	22·7(1·1)	68·5(1·9)	78·2(1·7)	79·1(2·1)	78·4(1·7)	78·3(1·7)
Other phases:	gl gt ru pl	gl gt	gl	gl gt	gt qz ru	gl gt qz ru	gl gt qz	gl gt qz
n:	8	16	10	11	11	13	13	19
SiO_2	48·90(42)	48·59(35)	50·08(36)	50·09(31)	50·96(47)	51·19(44)	50·02(35)	50·30(31)
TiO_2	2·12(14)	1·23(9)	0·74(6)	1·75(8)	1·94(15)	2·00(11)	1·87(8)	2·04(11)
Al_2O_3	10·98(26)	14·10(29)	11·46(37)	14·86(32)	15·66(67)	15·74(36)	15·09(20)	15·45(16)
FeO*	9·99(21)	7·76(16)	6·45(16)	8·03(20)	7·49(28)	7·51(17)	7·79(12)	7·77(15)
MnO	0·17(3)	0·17(3)	0·17(3)	0·13(3)	0·12(3)	0·14(5)	0·12(3)	0·11(4)
MgO	10·99(14)	11·51(17)	13·94(32)	9·34(19)	7·95(27)	7·85(19)	8·12(12)	8·11(12)
CaO	15·10(18)	15·57(57)	16·44(28)	13·94(27)	13·18(28)	13·00(17)	12·81(19)	13·04(18)
Na_2O	1·99(10)	2·02(8)	1·58(12)	2·97(11)	3·90(12)	3·91(14)	3·62(7)	3·77(10)
Sum	100·23(39)	100·95(32)	100·87(87)	101·10(28)	101·20(34)	101·34(28)	99·44(36)	100·59(42)
Mg no.	66·2	72·6	79·4	67·4	65·4	65·1	65·0	65·0
Components								
Ca-Eskola	0·043	0·029	0·014	0·101	0·118	0·131	0·120	0·11
Jadeite	0·141	0·141	0·110	0·206	0·269	0·269	0·255	0·262
Al-buffonite	0·117	0·067	0·040	0·094	0·104	0·107	0·102	0·110
CaTs	0·087	0·181	0·160	0·113	0·083	0·076	0·084	0·086
Diopside	0·369	0·339	0·425	0·277	0·256	0·246	0·251	0·250
En–Fs	0·244	0·234	0·251	0·210	0·170	0·172	0·188	0·183

Run no.:	A177-82	A177-96	A177-121	A171	A175	164	A195	A189
P (GPa):	3·0	3·0	3·0	3·0	3·0	3·0	3·0	3·0
T (°C):	1335	1335	1335	1350	1365	1375	1400	1425
t (h):	82	96	121	77	70·5	72·5	29	24
cpx (wt %):	76·3(1·6)	77·7(1·7)	78·7(1·6)	76·5(1·6)	76·6(1·7)	70·5(1·7)	65·3(1·7)	53·7(1·5)
Other phases:	gl gt qz	gl gt qz	gl gt qz	gl gt qz	gl gt qz	gl gt	gl gt	gl gt
n:	13	18	19	15	14	14	12	12
SiO_2	49·93(28)	50·77(33)	50·31(26)	50·08(22)	50·21(20)	49·94(27)	50·55(35)	49·93(39)
TiO_2	1·87(9)	2·02(8)	2·12(7)	1·79(7)	1·69(10)	1·49(10)	1·28(7)	0·96(6)
Al_2O_3	14·92(25)	15·46(23)	15·41(19)	14·86(15)	15·22(16)	14·78(18)	15·06(37)	14·60(20)
FeO*	7·73(12)	7·76(20)	7·73(11)	7·79(11)	7·69(12)	7·86(16)	7·63(23)	7·08(10)
MnO	0·11(4)	0·13(4)	0·11(4)	0·12(2)	0·12(3)	0·12(3)	0·13(4)	0·14(3)
MgO	8·27(10)	7·99(14)	7·96(12)	8·26(7)	8·27(14)	8·84(12)	9·31(15)	9·76(10)
CaO	13·05(12)	13·15(15)	13·10(13)	13·03(15)	12·80(13)	13·23(20)	13·70(22)	14·09(14)
Na_2O	3·55(10)	3·85(12)	3·78(9)	3·50(7)	3·46(7)	3·26(10)	3·23(10)	3·07(9)
Sum	99·44(26)	101·02(31)	100·54(33)	99·42(21)	99·44(24)	99·52(24)	100·90(39)	99·61(46)
Mg no.	65·6	65·0	64·7	65·4	65·7	66·7	68·5	71·1
Components								
Ca-Eskola	0·114	0·116	0·115	0·121	0·133	0·106	0·094	0·075
Jadeite	0·250	0·266	0·263	0·246	0·242	0·229	0·224	0·215
Al-buffonite	0·102	0·108	0·114	0·098	0·092	0·081	0·069	0·052
CaTs	0·086	0·080	0·080	0·085	0·090	0·107	0·124	0·140
Diopside	0·262	0·256	0·252	0·263	0·247	0·272	0·285	0·316
En–Fs	0·186	0·174	0·176	0·188	0·195	0·204	0·205	0·202

Run no.:	A190	A194	A197	A221K	A200K	A188K
P (GPa):	3·0	3·0	3·0	2·0	3·0	3·0
T (°C):	1450	1475	1500	1325	1275	1315
t (h):	19	12	2·5	46	96	91·5
cpx (wt %):	41·6(1·3)	35·6(1·5)	13·2(1·5)	46·3(8)	69·5(1·1)	69·2(1·0)
Other phases:	gl gt	gl gt	gl	gl gt	gl gt qz ru	gl gt qz
n:	17	18	8	15	17	12
SiO_2	49·66(17)	50·31(14)	49·69(53)	48·39(35)	50·91(33)	51·62(22)
TiO_2	0·85(4)	0·71(5)	0·69(20)	1·09(8)	1·87(13)	1·74(9)
Al_2O_3	14·49(16)	14·64(23)	13·79(50)	12·77(30)	14·29(25)	14·17(17)
FeO*	6·76(9)	6·24(13)	5·70(18)	7·90(22)	7·54(14)	7·34(12)
MnO	0·15(2)	0·14(3)	0·14(3)	0·16(3)	0·11(2)	0·10(3)
MgO	10·34(13)	11·12(23)	12·39(34)	11·94(25)	8·90(11)	8·71(9)
CaO	14·45(15)	14·88(18)	15·45(28)	15·81(23)	14·17(21)	13·65(21)
Na_2O	2·90(7)	2·67(11)	2·20(12)	1·81(9)	3·42(7)	3·49(7)
Sum	99·60(31)	100·71(27)	100·05(44)	99·88(40)	101·20(40)	100·82(35)
Mg no.	73·2	76·1	79·5	72·9	67·8	67·9
Components						
Ca-Eskola	0·058	0·064	0·043	0·018	0·101	0·133
Jadeite	0·203	0·185	0·153	0·128	0·236	0·241
Al-buffonite	0·046	0·038	0·037	0·060	0·100	0·093
CaTs	0·155	0·165	0·175	0·172	0·082	0·062
Diopside	0·330	0·334	0·361	0·378	0·309	0·298
En–Fs	0·208	0·215	0·231	0·244	0·172	0·171

Reported modes taken from Pertermann & Hirschmann (2003, table 2). Errors in parentheses for compositions and modes are one SD of the mean, reported as least units cited; 48·90(42) wt % SiO_2 should be read as 48·90 ± 0·42 wt %. *n*, number of points analyzed; FeO*, all Fe assumed to be FeO; Mg number is molecular Mg/(Mg + Fe) × 100. Details of cpx component calculations are given in text.

these conditions. The 2 GPa liquids plot along trends nearly parallel to those at 3 GPa, but displaced to higher MgO and CaO, and lower TiO_2, owing to the higher melt fraction at a given temperature. Na_2O shows relatively little variation throughout the melting interval, ranging from ~4 wt % near the solidus to ~3 wt % near the liquidus. This presumably reflects its relative compatibility in residual clinopyroxene ($D_{Na_2O}^{cpx/liq}$ ranges from 0·7 to 1·06). In contrast, K_2O changes significantly over the melting range at 3 GPa, from <0·1 wt % at 1425°C and above, to 0·8–1·4 wt % near the solidus.

Clinopyroxene

Aluminous clinopyroxene compositions vary systematically throughout the melting interval of G2 at 2–3 GPa (Table 4, Fig. 6). At 3 GPa, the Mg number is 65·1 at the solidus and increases to 79·3 at the liquidus; the range is similar at 2 GPa, from 66 to 79. CaO at 3 GPa varies from ~12·9 wt % at the solidus to 15·4 wt % just under the liquidus at 1500°C. At 2 GPa it increases from 15·1 to 16·3 wt % at 1250–1375°C. The exceptional aspect of the pyroxenes is the great enrichment in Al_2O_3. At 2 GPa, Al_2O_3 varies from 11 to 14 wt %, and is highest at 1325°C. But at 3 GPa, cpx has 15·5 wt % Al_2O_3 at the solidus, decreasing to 13·8 wt % just below the liquidus (Fig. 6). Cpx are also rich in TiO_2, and at constant pressure, TiO_2 decreases with rising temperature. TiO_2 is ~2 wt % near the solidus at 2 and 3 GPa. At 3 GPa, concentrations remain near-constant up to 1335°C, where rutile is present, then decrease markedly at higher temperature, where rutile is absent. With increasing pressure, cpx becomes significantly enriched in Na_2O. At 2 GPa, concentrations are 1·6–2·0 wt % Na_2O, but at 3 GPa they range from 3·9 wt % near the solidus down to 2·2 wt % at 1500°C.

Table 5: Composition of garnet and plagioclase

	Garnet							
Run no:	A284	A184	A202	166	A170	A168	A177-70	A177-82
P (GPa):	2·0	2·0	2·5	3·0	3·0	3·0	3·0	3·0
T (°C):	1250	1325	1325	1300	1315	1325	1335	1335
t (h):	82	40	60·5	92	96	92	70	82
Modal wt %:	12·6(1·1)	3·4(1·1)	11·3(1·1)	17·8(1·3)	17·4(1·3)	14·2(1·0)	15·5(1·1)	14·5(1·0)
Other phases:	gl cpx pl ru	gl cpx	gl cpx	cpx qz ru	gl cpx qz ru	gl cpx qz	gl cpx qz	gl cpx qz
n:	11	13	15	15	10	13	14	11
SiO_2	38·99(18)	39·89(21)	39·86(27)	39·28(16)	39·25(34)	39·07(22)	39·16(22)	38·85(42)
TiO_2	1·10(9)	0·80(12)	0·82(27)	0·81(26)	0·84(32)	1·01(15)	1·02(15)	0·97(13)
Al_2O_3	22·27(18)	23·20(25)	22·81(22)	22·62(24)	22·43(25)	22·41(17)	22·54(12)	22·31(22)
FeO*	19·62(22)	16·51(60)	18·86(31)	19·71(31)	19·64(33)	19·18(22)	19·59(22)	19·22(24)
MnO	0·47(3)	0·43(6)	0·43(4)	0·41(3)	0·41(3)	0·41(3)	0·44(6)	0·41(3)
MgO	10·84(17)	12·49(60)	10·38(28)	9·31(23)	9·40(25)	10·04(11)	9·81(27)	9·94(27)
CaO	6·96(20)	7·62(27)	8·14(38)	8·53(31)	8·53(32)	7·89(27)	8·31(28)	7·94(24)
Na_2O	0·05(3)	0·07(7)	0·08(3)	0·12(3)	0·11(3)	0·13(3)	0·12(4)	0·11(2)
Sum	100·30(39)	101·01(33)	100·88(51)	100·81(52)	100·62(54)	100·13(36)	100·98(37)	99·75(39)
Mg no.	49·6	57·4	49·5	45·7	46·0	48·3	47·2	48·0
Components								
Almandine	0·405	0·336	0·390	0·412	0·410	0·402	0·406	0·403
Spessartine	0·013	0·011	0·011	0·011	0·011	0·011	0·012	0·011
Pyrope	0·399	0·453	0·383	0·347	0·350	0·375	0·362	0·372
Grossular	0·184	0·199	0·216	0·229	0·228	0·212	0·220	0·214

	Garnet							
Run no.:	A177-96	A177-121	A171	A175	164	A195	A189	A190
P (GPa):	3·0	3·0	3·0	3·0	3·0	3·0	3·0	3·0
T (°C):	1335	1335	1350	1365	1375	1400	1425	1450
t (h):	96	121	77	70·5	72·5	29	24	19
Modal wt %:	16·3(1·1)	16·1(1·1)	14·0(1·0)	13·3(1·1)	11·6(1·0)	10·9(1·2)	9·9(1·0)	7·7(9)
Other phases:	gl cpx qz	gl cpx qz	gl cpx qz	gl cpx qz	gl cpx	gl cpx	gl cpx	gl cpx
n:	11	15	10	12	14	15	11	13
SiO_2	39·82(35)	39·49(29)	39·15(29)	39·09(26)	38·43(21)	39·80(22)	39·90(22)	39·39(24)
TiO_2	1·02(14)	1·01(14)	0·81(22)	0·96(16)	1·00(15)	0·95(11)	0·85(11)	0·67(20)
Al_2O_3	22·83(24)	22·76(24)	22·48(17)	22·53(20)	22·09(14)	22·93(17)	22·39(21)	22·64(17)
FeO*	19·72(22)	19·62(22)	18·92(28)	18·85(25)	18·50(30)	18·41(30)	16·53(23)	15·82(42)
MnO	0·43(6)	0·43(6)	0·39(3)	0·40(3)	0·41(3)	0·40(4)	0·40(3)	0·41(6)
MgO	10·00(17)	9·86(17)	9·86(24)	10·11(22)	10·39(23)	10·84(26)	11·50(28)	11·77(46)
CaO	8·26(17)	8·30(17)	8·06(35)	8·21(27)	8·13(37)	8·31(32)	8·27(30)	8·62(37)
Na_2O	0·11(2)	0·14(2)	0·09(2)	0·10(3)	0·10(3)	0·11(2)	0·08(2)	0·09(3)
Sum	102·20(59)	101·63(59)	99·77(28)	100·25(47)	99·05(38)	101·75(24)	99·91(44)	99·42(38)
Mg no.	47·5	47·3	48·2	48·9	50·0	51·2	55·4	57·0
Components								
Almandine	0·405	0·405	0·400	0·393	0·386	0·376	0·343	0·327
Spessartine	0·012	0·012	0·011	0·011	0·011	0·011	0·011	0·011
Pyrope	0·366	0·363	0·371	0·376	0·386	0·395	0·426	0·434
Grossular	0·217	0·22	0·218	0·219	0·217	0·218	0·220	0·228

	Garnet				Plagioclase
Run no.:	A194	A221K	A200K	A188K	A284
P (GPa):	3·0	2·0	3·0	3·0	2·0
T (°C):	1475	1325	1275	1315	1250
t (h):	12	46	96	91·5	82
Modal wt %:	4·5(1·0)	2·3(7)	15·8(6)	16·0(6)	21·2(1·2)
Other phases:	gl cpx	gl cpx	gl cpx qz ru	gl cpx qz	gl cpx gt ru
n:	11	11	10	12	9
SiO_2	40·21(20)	39·41(22)	39·53(39)	39·40(19)	59·93(19)
TiO_2	0·72(9)	0·76(8)	0·85(20)	0·88(14)	0·13(3)
Al_2O_3	23·06(17)	22·98(25)	22·57(27)	22·47(24)	25·65(28)
FeO*	13·91(35)	15·88(31)	19·17(25)	18·56(18)	0·53(9)
MnO	0·38(3)	0·44(4)	0·43(3)	0·41(4)	0·03(3)
MgO	13·50(39)	13·05(33)	9·85(24)	10·02(17)	0·08(5)
CaO	7·76(20)	7·27(27)	8·45(29)	8·62(25)	7·22(16)
Na_2O	0·07(2)	0·05(3)	0·12(3)	0·12(3)	6·93(11)
Sum	99·61(28)	99·86(40)	100·97(57)	100·48(50)	100·49(35)
Mg no.	63·4	9·4	47·8	49·0	
Components					
Almandine	0·287	0·324	0·398	0·387	
Spessartine	0·010	0·012	0·012	0·011	
Pyrope	0·497	0·474	0·365	0·372	
Grossular	0·205	0·190	0·225	0·230	

Reported modes taken from Pertermann & Hirschmann (2003, table 2). Errors in parentheses for compositions and modes are one SD of the mean, reported as least units cited; 38·99(18) wt % SiO_2 should be read as 38·99 ± 0·18 wt %. *n*, number of points analyzed; FeO*, all Fe assumed to be FeO; Mg number is molecular Mg/(Mg + Fe) × 100. Details of garnet component calculations are given in text.

The stoichiometry of cpx was obtained by assuming all Fe exists as FeO, which is probable, given the reducing conditions of the graphite-lined capsules. For the 2·0 GPa runs, the calculated cation totals are 3·98–3·99 for six oxygen anions, but at higher pressures the totals are as low as 3·93. This cation deficiency is genuine, as analysis of well-characterized omphacite (USNM 110607) and Cr-augite (USNM 164905) secondary standards yielded average cation totals of 3·991 and 4·004, respectively.

The cpx components are calculated as follows. All Ti is assumed to exist as $CaMg_{0.5}Ti_{0.5}AlSiO_6$ (alumino-buffonite, Sack & Ghiorso, 1994) and all Na is apportioned to $NaAlSi_2O_6$ (Jadeite, Jd). The remaining tetrahedral Al is then assigned to $CaAl_2SiO_6$ (Ca-Tschermaks, CaTs). The cation deficiency is best reconciled by the presence of the Ca-Eskola component (CaEs, $Ca_{0.5}[\ ]_{0.5}AlSi_2O_6$; Smyth, 1980; McCormick, 1986). The remaining Ca is then assigned to $CaMgSi_2O_6$ (Diopside, Di), and the residual Mg and Fe are expressed as $(Mg, Fe)_2Si_2O_6$ (Enstatite–Ferrosilite, En–Fs) solid solution. Up to 14% CaEs component is present in the 3·0 GPa runs, indicating that as much as 7% of cpx M2-site may be vacant.

Garnet

Garnet compositions are given in Table 5 and illustrated in Fig. 7. The Mg number of garnets increases steadily with rising temperature. At 3 GPa, it increases from 45·4 at the solidus to 63·0 at 1475°C, the highest temperature at which garnet is observed. At 2 GPa the Mg number is 49·3 at 1250°C, increasing to 57·1 at 1325°C. The higher Mg number of garnet at a given temperature at lower pressure is probably attributable to the mass balance imposed by greater melt fractions. CaO contents of garnets are greater at high pressure: 7·0–7·5 wt % at 2 GPa and 7·8–8·7 wt % at 3 GPa. No systematic variations of CaO with temperature are apparent at 3 GPa. Garnets are generally elevated in

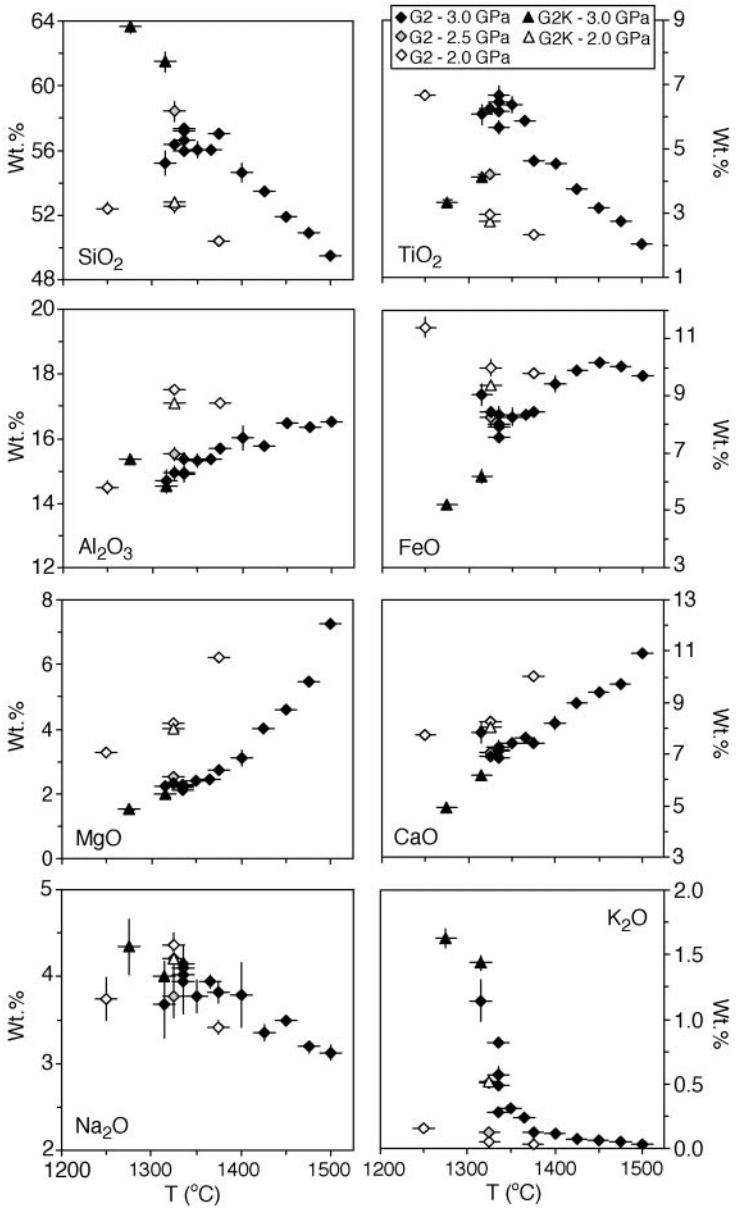

Fig. 5. Compositions of partial melts from G2 eclogite partial melting experiments. Error bars are ±12°C and ±1 SD (wt %); the error is less than the size of symbols where error bars are not shown. Partial melts with added K_2O in the starting material (G2K) have markedly elevated SiO_2 contents compared with the nearly K-free experiments (G2).

TiO_2, ranging from 0·7 to 1·1 wt % overall (Fig. 7). As with cpx, TiO_2 in garnet is near-constant when rutile is present, and diminishes as temperature rises beyond rutile-out at 1335–1350°C.

DISCUSSION

Mineral modes and melting reactions

The predominant mineral throughout the melting range of G2 is cpx. Garnet constitutes only 18 wt % of the mode near the solidus, and is reduced in abundance with rising temperature. The highly aluminous cpx composition is similar to the G2 bulk composition, thus requiring little garnet for mass balance. Despite its small near-solidus mode, garnet remains stable throughout most of the melting interval, persisting to within ~25–50°C of the liquidus. Takahashi & Nakajima (2002) also reported garnet persisting to near-liquidus conditions at 2·7–3 GPa for their 'Archaean MORB' bulk composition. Johnston (1986) found somewhat higher garnet modes (i.e. 16% at

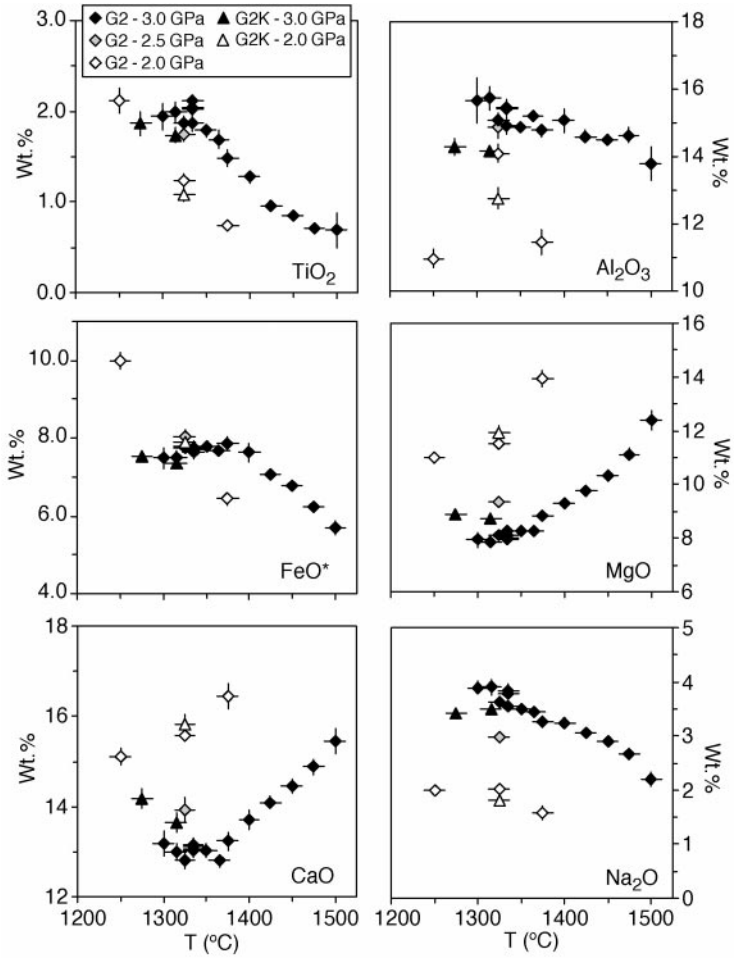

Fig. 6. Composition of clinopyroxene from G2 eclogite partial melting experiments. Error bars are ±12°C and ±1 SD (wt %); the error is less than the size of symbols where error bars are not shown. The overall elevated Al_2O_3 content of the cpx at 3·0 GPa should be noted. Cpx components are given in Table 4 (see discussion of cpx chemistry for further details).

$F = 33\%$), presumably owing to the more aluminous bulk composition in that study. Similarly, Yaxley & Green (1998) found ~27% garnet in the near-solidus region, partly owing to their more aluminous bulk composition and to the higher pressures (3·5 GPa) of their experiments.

We use the approach of Walter *et al.* (1995) to obtain the average melting reactions of our 3 GPa experiments in terms of mass units:

$$0{\cdot}283\ \text{cpx} + 0{\cdot}462\ \text{gt} + 0{\cdot}213\ \text{qz} + 0{\cdot}042\ \text{ru} = 1{\cdot}000\ \text{liq (solidus to ru-out)} \quad (1)$$

$$0{\cdot}588\ \text{cpx} + 0{\cdot}229\ \text{gt} + 0{\cdot}184\ \text{qz} = 1{\cdot}000\ \text{liq (ru-out to qz-out)} \quad (2)$$

$$0{\cdot}872\ \text{cpx} + 0{\cdot}173\ \text{gt} = 1{\cdot}000\ \text{liq (qz-out to grt-out)}. \quad (3)$$

As equations (1)–(3) indicate, garnet and cpx are the principal contributors to melt formation near the solidus. With increasing melt fraction, the garnet contribution diminishes significantly and cpx becomes the predominant mineral. This shift explains the persistence of garnet towards higher temperatures: while the initial garnet mode is low, its contribution to partial melts is also small. The high contribution of cpx (0·87) near the liquidus stems in part from the cpx composition, which approaches that of the G2 starting material under these conditions.

Melt composition, quartz and rutile saturation

It is commonly assumed that anhydrous partial melts of basaltic eclogite are dacitic (e.g. Hauri, 1996), but the glasses in our G2 experiments range from basaltic at high temperature to andesitic at low temperature (Fig. 5). In detail at 3 GPa, SiO_2

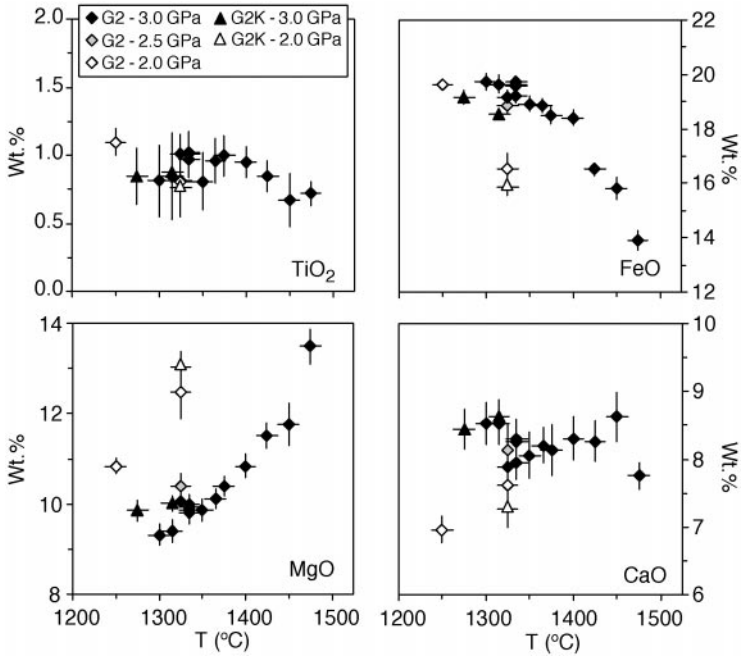

Fig. 7. Composition of garnet from G2 eclogite partial melting experiments. Error bars are ±12°C and ±1 SD (wt %); the error is less than the size of symbols where error bars are not shown. (Note the relatively small variations in CaO and TiO_2, whereas the Mg number increases with rising temperatures, as evidenced by increasing MgO and decreasing FeO*.) The garnet components are given in Table 5 (see text for details).

increases from the liquidus down to quartz saturation at 1365°C, at which point it becomes nearly constant. Quartz saturation fixes the silica activity (a_{SiO_2}), which means that silica concentration in the liquid can be enhanced only by agents that diminish the activity coefficient (γ_{SiO_2}) (e.g. Ryerson, 1985; Hirschmann *et al*., 1998).

In contrast, Yaxley & Green (1998) found dacitic glasses (63–65 wt % SiO_2) coexisting with coesite at 3·5 GPa from dry partial melting experiments on a composition (GA1) similar to G2 (Table 1). These dacitic glasses are more potassic (3·6–3·8 wt % K_2O) than the G2 partial melts, which have no more than 1·1 wt % K_2O (Fig. 8). Similarly, Klemme *et al*. (2002) found dacitic glasses with high (4·8–6·9 wt %) K_2O in partial melting experiments at 3 GPa using a model (FeO-free) eclogite (SBM6). The differences are attributable to bulk composition: we assumed that subduction processes remove most K_2O from recycled crust (Kogiso *et al*., 1997*a*, 1997*b*) and so G2 was intended to be nearly K_2O-free (~0·03 wt %), whereas GA1 and SBM6 have 0·44 and 1·2 wt % K_2O, respectively. Because alkalis lower γ_{SiO_2} in polymerized melts (Kushiro, 1975; Hirschmann *et al*., 1998), G2 should form less silicic quartz- or coesite-saturated partial melts.

To test this hypothesis, we performed additional experiments with a modified G2 composition. We added a small amount of potassium silicate (crystallized from a gel) to create G2K (Table 1), which has 0·26 wt % K_2O. G2K has slightly more SiO_2 than G2, but because both compositions have modal quartz at subsolidus conditions, this simply increases the near-solidus quartz mode by a small amount and should not affect melt compositions.

Experiments with G2K at 3 GPa and 1315 and 1275°C (runs A188K and A200K, respectively) produced cpx, garnet, quartz and glass; rutile was detected at 1275°C. Glass, cpx and garnet compositions are given in Tables 3, 4 and 5, respectively. Although these experiments were conducted near or below the solidus of unadulterated K-poor G2, the melt fractions, calculated from mass balance, are 14·5 ± 1·1% and 14·3 ± 0·9% at 1315 and 1275°C, respectively. Alternative calculations from the K_2O content of the quenched glass, assuming perfect incompatibility of K, yield 18 and 16%, respectively. Thus, K_2O acts as a flux, increasing the melt fraction and lowering the solidus (Hirschmann *et al*., 1998; Hirschmann, 2000).

The G2K glasses have 1·4–1·6 wt % K_2O, and, as anticipated, they are enriched in SiO_2 (61–64 wt %, Table 3, Fig. 8) relative to those from partial melts of G2. The effect of K_2O on SiO_2 evident in the comparison between the experiments with G2 and G2K is surprisingly large; i.e. the G2K partial melts have just

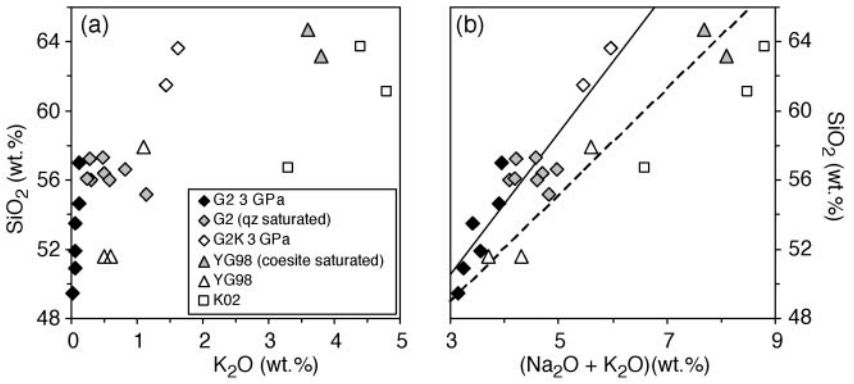

Fig. 8. Effect of (a) K_2O and (b) total alkalis on silica content of G2 and G2K partial melts of eclogite at 3 GPa, compared with 3 GPa partial melts of synthetic FeO-free SBM6 eclogite (Klemme *et al*., 2002) (K02) and 3·5 GPa partial melts of GA1 eclogite (Yaxley & Green, 1998) (YG98). Quartz or coesite (at 3·5 GPa) saturated compositions are indicated with shaded symbols. The small increase in K_2O in G2K partial melts relative to those from G2 has a substantial effect on silica concentrations, partly because of related shifts in TiO_2 concentrations (see text). Silica correlates with total alkali content, but, owing to different bulk compositions and pressures, different trends are apparent for each study.

0·6–0·8% more K_2O than the most potassic quartz-saturated G2 partial melts, but 4–7 wt % more SiO_2. Apparently, the enrichment of SiO_2 in the G2K glasses is enhanced by the combined effect of lower temperature and reduced TiO_2 in these glasses (Table 3), as TiO_2 increases the silica activity in melts (Xirouchakis *et al*., 2001). We will return to this point after a discussion of rutile saturation in near-solidus eclogites.

At a given total alkali ($Na_2O + K_2O$) content, the G2 and G2K partial melts have more SiO_2 than partial melts from the studies of Yaxley & Green (1998) or Klemme *et al*. (2002) (Fig. 8). The liquids in the experiments of Klemme *et al*. (2002) are not saturated in quartz, presumably because a_{SiO_2} is diminished by the extreme alkali concentration. Differences in SiO_2 content at a given alkali content between the 3 GPa experiments with G2 and G2K and the 3·5 GPa experiments with GA1 (Yaxley & Green, 1998) probably reflect a decrease in the SiO_2 content of silica-saturated liquids with increasing pressure (Gaetani *et al*., 1998), the fact that the GA1 experiments are saturated in coesite rather than quartz, and possibly the effects of other differences in bulk composition between G2/G2K and GA1.

The presence of rutile during partial melting of eclogite buffers the TiO_2 activity in the liquid and therefore influences the character of near-solidus partial melts. It also affects distributions of high field strength elements (HFSE) during near-solidus partial melting (e.g. Foley *et al*. 2000). At 3 GPa, rutile is inferred to be saturated from the solidus of G2 to 1335°C, coexisting with glasses with 5·7–6·7 wt % TiO_2. The modified G2K starting material has rutile at 1275°C and 3 GPa, coexisting with glass containing only 3·3 wt % TiO_2 (Fig. 9). This behavior is distinct from that of rutile-saturated peralkaline melts, where increasing K_2O correlates positively with the TiO_2 concentration necessary to achieve rutile saturation (Hess, 1995). However, the glasses in G2K experiments contain much more SiO_2 than their G2 counterparts, and this probably has a critical influence on the TiO_2 concentration in rutile-saturated glasses (Ryerson & Watson, 1987).

Our experiments, combined with other eclogite partial melting experiments at comparable pressures, suggest that high-pressure andesitic liquids require 5–7 wt % TiO_2 to be saturated in rutile. More silicic liquids require progressively less TiO_2, such that dacitic liquids may be rutile saturated with only ~1 wt % TiO_2 (Fig. 9). These observations are in close agreement with the rutile-saturation model of Ryerson & Watson (1987) (Fig. 9). We have argued that increases in TiO_2 diminish the amount of SiO_2 needed to saturate liquids in quartz and that increases in SiO_2 diminish the amount of TiO_2 needed to saturate liquids in rutile. Thus it is apparent that combined rutile and quartz saturation can occur either in low-silica, high-TiO_2 liquids or in high-SiO_2, low-TiO_2 liquids. These relationships result because SiO_2 and TiO_2 do not tend to form Si–O–Ti linkages in silicate liquids; instead, they self-polymerize as Si–O–Si and Ti–O–Ti, thereby raising each other's activity coefficient (Hess, 1995; Xirouchakis *et al*., 2001). There may appear to be some circularity to this effect, as SiO_2–TiO_2 interactions cannot explain which rutile + quartz-saturated liquids will be SiO_2-rich and TiO_2-poor and which will be the opposite. The answer lies in independent variables such as alkali content and temperature, which influence the SiO_2 or TiO_2 contents of saturated liquids. Thus, high-temperature, alkali-poor liquids will be relatively SiO_2-poor and TiO_2-rich, and

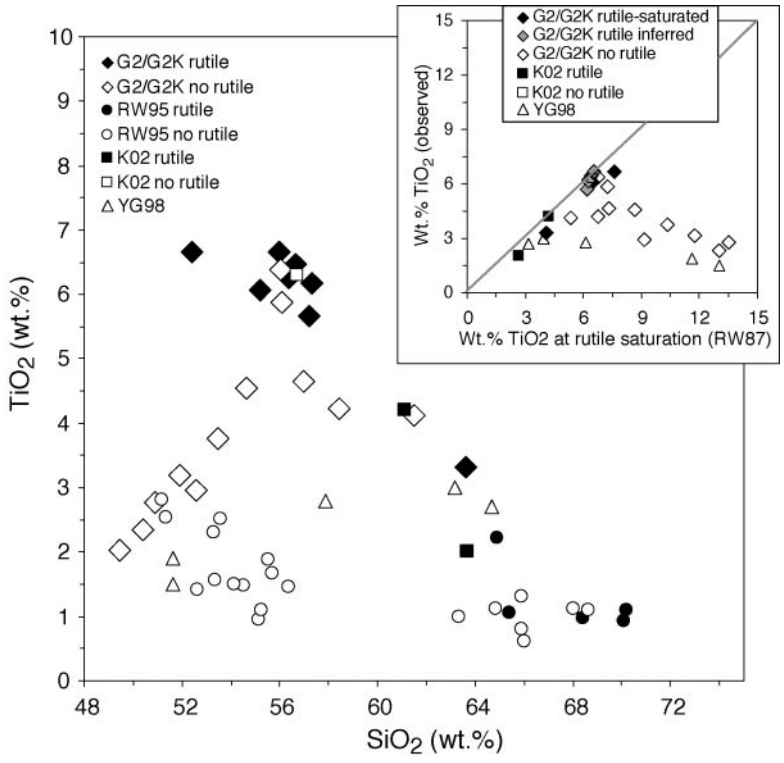

Fig. 9. Observed rutile saturation for G2 and G2K eclogite partial melts at 2–3 GPa vs SiO_2 in silicate liquid and from the experiments of Yaxley & Green (1998) (YG98), Klemme *et al.* (2002) (K02) and from the experiments between 2·2 and 3·2 GPa of Rapp & Watson (1995) (RW95). Filled symbols represent runs in which rutile was observed or in which rutile was not observed but saturation is inferred, and open symbols are from experiments in which rutile is not stable. For this range of bulk compositions and pressures, the decrease in TiO_2 required for rutile saturation with increasing SiO_2 produces a fairly consistent trend. Inset compares TiO_2 observed in silicate liquids with that predicted for rutile saturation by the model of Ryerson & Watson (1987) (RW87). Observed rutile saturation shows close agreement with the predictive model: runs that show rutile or are near rutile saturation plot very close to the 1 : 1 line, and clearly rutile-undersaturated runs deviate systematically to high predicted TiO_2 concentrations whereas actual measured concentrations approach those of the G2 or G2K starting compositions. The shift of rutile saturation to lower temperature in the G2K experiments where partial melts are more SiO_2-rich should be noted.

low-temperature, alkali-rich ones will be SiO_2-rich and TiO_2-poor.

Interactions between alkalis, TiO_2 and SiO_2 in rutile + quartz-saturated melts can be understood from examination of a simple thermodynamic model, as illustrated in Fig. 10. The model assumes that SiO_2 and TiO_2 have positive non-ideal interactions, meaning that these oxides raise the activity coefficients of each other, and that SiO_2 and K_2O have negative non-ideal interactions, meaning that K_2O depolymerizes silicate networks and reduces the activity coefficient of silica (Kushiro, 1975; Ryerson, 1985; Hirschmann *et al.*, 1998; Xirouchakis *et al.*, 2001). Although the model assumes that K_2O–TiO_2 interactions are ideal, addition of K_2O to the system lowers the TiO_2 of rutile-saturated melts indirectly by raising the SiO_2 content required to maintain quartz saturation; the increase in SiO_2 increases the activity coefficient of TiO_2. The consequent lowering of the TiO_2 in the melts further reduces the activity coefficient of silica, thereby raising the SiO_2 concentration of the liquid required to maintain quartz saturation. It should be noted that the calculation is performed for two hypothetical scenarios—one corresponding to the low-temperature case, in which the TiO_2 concentration required for rutile saturation is low, and the other corresponding to the high-temperature case, with higher TiO_2 concentrations in the liquid. In the former case, addition of K_2O has relatively little effect on liquid TiO_2, and the aggregate effect on SiO_2 is principally that of K_2O alone. In the latter case, K_2O affects SiO_2 both directly and indirectly through TiO_2, and the same increment of K_2O addition has a more pronounced effect on liquid SiO_2 content. This is precisely what is observed in the comparison between the G2 and G2K experiments.

Recently, Klemme *et al.* (2002) parameterized rutile saturation during eclogite partial melting at 3 GPa in terms of bulk TiO_2 concentration and melt fraction. They concluded that relatively high degrees of melting

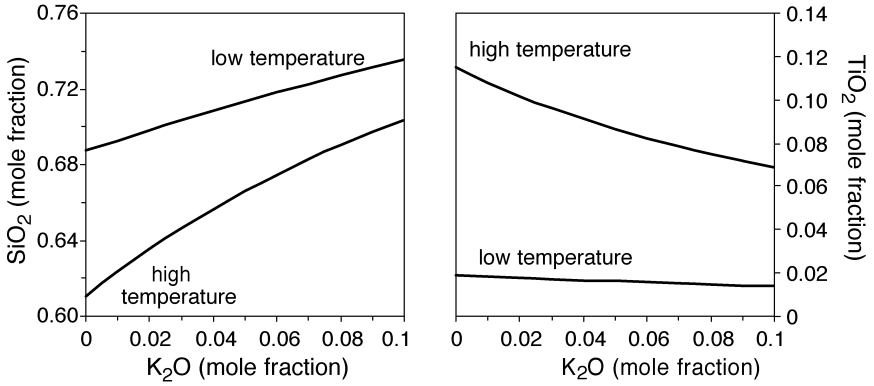

Fig. 10. Simple thermodynamic model illustrating the combined effects of SiO_2–TiO_2–K_2O on the SiO_2 and TiO_2 content of quartz + rutile-saturated liquids. The calculation is based on a four-component solution SiO_2–TiO_2–K_2O–X (X = Al_2O_3, MgO, CaO, etc.) using a symmetric regular solution formulation [see Hirschmann *et al.* (1998) for analytic expressions] and assumes that SiO_2–TiO_2 interactions increase the enthalpy of mixing ($W_{SiO_2-TiO_2}$ = 40 kJ) and that SiO_2–K_2O interactions diminish it ($W_{SiO_2-K_2O}$ = −30 kJ). TiO_2–K_2O interactions and all interactions with component X are assumed to be ideal. Calculations are shown for cases in which TiO_2 solubility in the liquid is assumed to be low and high, corresponding to low- and high-temperature conditions, respectively (Ryerson & Watson, 1987). Increases in K_2O in the liquid enhance the SiO_2 concentration of quartz-saturated liquids, as is well known from experiments (Kushiro, 1975; Ryerson, 1985; Hirschmann *et al.*, 1998). In turn, increases in SiO_2 diminish the solubility of TiO_2, and conversely, decreases in TiO_2 increase the solubility in SiO_2. It should be noted that the effect on SiO_2 is greater for the 'high-temperature' case, where TiO_2 solubility is greater and therefore changes in liquid TiO_2 are more pronounced.

are required to exhaust rutile from eclogite residua and their model predicts retention of rutile until nearly 40% melting for a bulk rock with a TiO_2 concentration (2 wt %) similar to G2. In contrast, we find that rutile is exhausted from the residue of G2 after only ∼8% partial melting. For G2K, which has a TiO_2 concentration comparable with G2, rutile is exhausted at ∼15% melting. As is clear from the above discussion, the chief difference in rutile stability between G2 and G2K is that the latter, being more potassic, generates more silicic partial melts. The relative ease with which rutile is exhausted from eclogite sources suggests that magmas with strong rutile signatures (i.e. high Zr/Nb, Foley *et al.*, 2000) are produced from anhydrous eclogitic sources only at relatively low melt fraction or from bulk compositions with unusually high K_2O. The parameterization of Klemme *et al.* (2002) probably is applicable only to the latter case.

Partitioning of Ti and Na between cpx, garnet and silicate liquid

The Na and Ti concentrations of mafic lavas are useful indicators of the lithologies and extent of melting in magma source regions (Langmuir *et al.*, 1992; Putirka, 1999) and are influenced by mineral–melt partitioning. In this section we review partitioning of these elements between cpx, garnet and silicate liquid from our experiments and related studies.

At 3 GPa, the partition coefficient for Na between cpx and silicate liquid, $D_{Na_2O}^{cpx/liq}$, ranges between 0·7 and 1·06, with larger values predominating at low temperature and smaller values at high temperature (Fig. 11). At 2 GPa, values for $D_{Na_2O}^{cpx/liq}$ are smaller (0·43–0·53). A positive correlation with pressure and a broad trend of diminished $D_{Na_2O}^{cpx/liq}$ with rising temperature is also observed in previous measurements for $D_{Na_2O}^{cpx/liq}$ in dry and hydrous eclogitic systems at 2–3·5 GPa (Fig. 11). These relations are qualitatively consistent with the empirical parameterization of Blundy *et al.* (1995), but the latter incorporates a much stronger temperature dependence for $D_{Na_2O}^{cpx/liq}$ than is observed for eclogitic systems in this pressure interval (Fig. 11). This presumably reflects the relative simplicity of the Blundy *et al.* (1995) parameterization.

For partitioning of Ti between cpx, garnet and silicate liquid in the G2 partial melting experiments, $D_{TiO_2}^{cpx/liq}$ and $D_{TiO_2}^{cpx/gt}$ are strongly temperature dependent, but $D_{TiO_2}^{gt/liq}$ is not (Fig. 12). For the experiments at 3 GPa, $D_{TiO_2}^{cpx/liq}$ and $D_{TiO_2}^{cpx/gt}$ can be fitted to the following equations:

$$D_{TiO_2}^{cpx/liq} = -4{\cdot}304 + 5246/T\ (\mathrm{K}) \qquad (4a)$$

$$D_{TiO_2}^{cpx/gt} = -7{\cdot}173 + 12591/T\ (\mathrm{K}). \qquad (4b)$$

These apparent temperature dependences are likely to stem in part from changes in phase composition with progressive melting (e.g. Figs 5–7). Temperature dependences of $D_{TiO_2}^{cpx/liq}$ and $D_{TiO_2}^{cpx/gt}$ are also evident when the G2 data are combined with data from other experimental studies relevant to anhydrous partial melting of pyroxenite and peridotite between 2 and

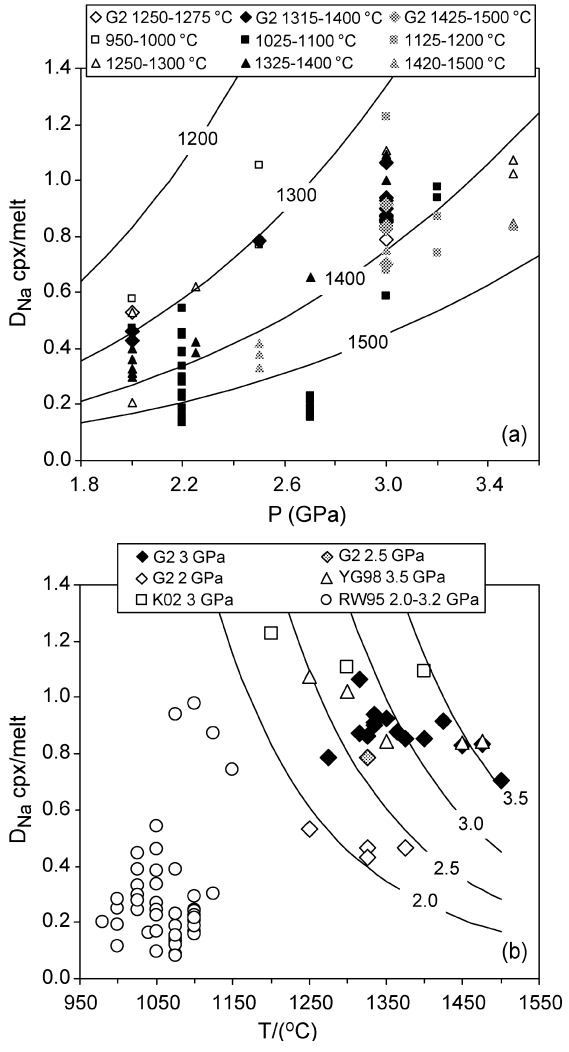

Fig. 11. Partitioning of Na_2O between cpx and glass for the G2 partial melting experiments and from studies relevant to hydrous and anhydrous eclogite and pyroxenite partial melting in the range of pressures between 2 and 3·5 GPa. Experiments were grouped in (a) temperature and (b) pressure ranges and compared with the model for Na partitioning between cpx and liquid given by equation (16) of Blundy *et al.* (1995). As indicated by the model, $D^{cpx/liq}_{Na_2O}$ increases with increasing pressure and decreases with rising temperature, but the model indicates much greater temperature dependence than found in the experiments. Anhydrous eclogite and pyroxenite partial melting data are from Takahashi *et al.* (1998), Yaxley & Green (1998) (YG98), Klemme *et al.* (2002) (K02), Takahashi & Nakajima (2002), Hirschmann *et al.* (2003) and this study. The bulk of the hydrous eclogite melting data is from Rapp & Watson (1995) (RW95), at pressures of 2·2, 2·7 and 3·2 GPa and 950–1100°C; additional data are taken from Green *et al.* (2000) and Klein *et al.* (2000). Consequently, (a) shows mostly anhydrous melting experiments, and in (b) the data for hydrous melting cluster at low temperature, despite their 2·2–3·2 GPa pressure range.

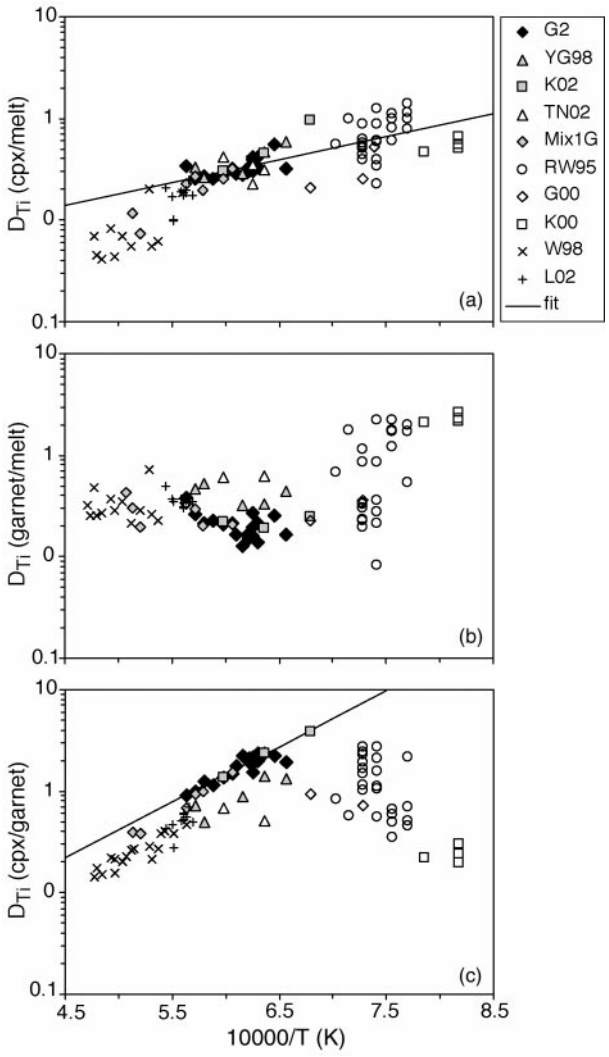

Fig. 12. Partitioning of TiO_2 between (a) cpx and glass, (b) garnet and glass, and (c) cpx and garnet for the G2 partial melting experiments vs temperature. Also shown are experimental data relevant to anhydrous partial melting of quartz eclogite between 2 and 3·5 GPa (YG98, Yaxley & Green, 1998; K02, Klemme *et al.*, 2002; TN02, Takahashi & Nakajima, 2002), garnet pyroxenite between 2 and 5 GPa (Mix1G, Hirschmann *et al.*, 2003; Kogiso *et al.*, 2003), hydrous partial melting of quartz eclogite between 2 and 3 GPa (RW95, Rapp & Watson, 1995; G00, Green *et al.*, 2000; K00, Klein *et al.*, 2000), and peridotite between 2·8 and 7 GPa (W98, Walter, 1998; L02, Longhi, 2002). Cpx–melt and cpx–garnet partition coefficients display significant correlations with temperature and the linear regressions for ln K_D vs $10^4/T$ from equation (4) are shown for the 3 GPa subset of experiments from this study.

7 GPa, although the slope of the overall trend is steeper than that determined from our 3 GPa experiments alone (Fig. 12). The differences in slope may reflect uncertainties and data scatter, or they may reflect more profound variations in composition and pressure with temperature, thereby enhancing the apparent temperature dependence of $D^{cpx/liq}_{TiO_2}$ and $D^{cpx/gt}_{TiO_2}$.

Interestingly, relations for $D^{cpx/liq}_{TiO_2}$, $D^{gt/liq}_{TiO_2}$ and $D^{cpx/gt}_{TiO_2}$ from experiments relevant to hydrous partial melting of eclogite (Rapp & Watson, 1995; Green *et al.*, 2000;

Klein *et al*., 2000) are distinct from trends defined by the anhydrous experiments (Fig. 12). Hydrous and anhydrous values for $D_{TiO_2}^{cpx/liq}$ plot along the same general trend, but in hydrous experiments $D_{TiO_2}^{gt/liq}$ extend to values >1 and $D_{TiO_2}^{cpx/gt}$ diminish with falling temperature (increasing $1/T$). The larger observed values of $D_{TiO_2}^{gt/liq}$ correspond to SiO_2-rich (>65 wt % SiO_2) hydrous liquids, suggesting that the effect is a consequence of higher activity coefficients of TiO_2 in such liquids, but this does not explain why a similar effect is not observed for $D_{TiO_2}^{cpx/liq}$. Perhaps there are also distinct compositional features of cpx coexisting with these highly silicic hydrous liquids that similarly raise the activity coefficient of titaniferous pyroxene species, thereby making garnet a more important reservoir for TiO_2 in hydrous eclogite systems. Although a detailed exploration of these differences is beyond the scope of this study, these observations suggest that trace element partition coefficients determined for the anhydrous eclogite system may not be applicable to partial melting of hydrous eclogite.

Comparison with previous studies, anhydrous and hydrous

In Fig. 13 we compare the nominally anhydrous partial melts of eclogite from this study with those from Takahashi *et al*. (1998), Yaxley & Green (1998) and Takahashi & Nakajima (2002), and with the hydrous partial melts of eclogite from Rapp & Watson (1995). All of these studies were performed on silica-saturated basaltic eclogites and we restrict our attention to experiments conducted between 2 and 3·5 GPa. Despite some differences in bulk composition (Table 1), there are broad similarities in the compositional trends. When plotted against MgO, SiO_2, FeO* and CaO plot on similar trends, although the hydrous experiments extend to lower MgO, FeO* and CaO and higher SiO_2. The more extreme compositions of hydrous partial melts largely reflect the stabilizing effect of H_2O on silicate liquid, which allows melt formation at lower temperature. TiO_2 concentrations vary substantially, consistent with the discussion in the previous section. Low TiO_2 contents of hydrous partial melts are in some cases a consequence of low TiO_2 in some of the bulk compositions employed by Rapp & Watson (1995), but are also a consequence of low rutile solubility at low temperature (Ryerson & Watson, 1987). Hydrous partial melts are also systematically richer in Al_2O_3, probably owing to diminished activity of aluminosilicate components effected by dissolved H_2O (e.g. Sykes & Kubicki, 1994). The high Na_2O in some of the experiments of Rapp & Watson (1995) reflects the high Na_2O (4·33 wt %) in one of the starting compositions used in that study.

One distinction evident in the trend of MgO vs SiO_2 is that the partial melts generated by Takahashi *et al*. (1998) and Takahashi & Nakajima (2002) are systematically richer in SiO_2 at a given MgO content than those from the other studies. This distinction could reflect bulk composition effects. For example, the low bulk TiO_2 in the composition employed by Takahashi & Nakajima (2002) may enhance SiO_2, although TiO_2-poor partial melts from other studies do not show a similar SiO_2–MgO trend (Fig. 13). However, poor mass balances between reported phase and bulk compositions of Takahashi *et al*. (1998) and Takahashi & Nakajima (2002) suggest that the high SiO_2 contents reported for glasses in these two studies could be analytical artifacts (Fig. 14).

The garnet–dacite connection

A requirement for formation of significant fractions of silica-rich partial melts from basaltic bulk compositions is that the mineral residue must be much less siliceous than the bulk composition. Because the silica content of high-pressure eclogitic cpx tends to be similar to that of typical basalt (48–52 wt %, Table 3; see also Rapp & Watson, 1995; Yaxley & Green, 1998; Takahashi & Nakajima, 2002), generation of appreciable fractions of high-silica liquid requires significant garnet in the residue (Fig. 15) (although amphibole may also play a role in hydrous systems). There is no specific relationship between the required mode of garnet and the allowable mass of silicic (>60 wt % SiO_2) partial melt, as mass balances are affected by the details of bulk-rock and cpx compositions, and by the presence of other phases such as feldspar or quartz–coesite. However, a general rule of thumb is that the mass of dacitic partial melt generated should not be greater than the mass of garnet present in the residue at that melt fraction. Thus, one can expect that dacitic partial melts of eclogite will carry significant garnet signatures in their REE patterns. We note that correlations between silica and garnet signatures, which are expected for garnet pyroxenite sources, are the opposite of what one would expect for peridotite sources. In peridotite partial melting, high silica generally reflects low-pressure melt–solid separation, and strong garnet signatures reflect high-pressure melt–solid separation of low-silica melts (Frey *et al*., 1994).

Eclogite in the source of Koolau, Hawaii?

Following the suggestion of Hauri (1996), the possibility that the lavas from Koolau, Hawaii, derive in part from partial melts of recycled eclogite has received considerable attention. In addition to distinct isotopic characteristics (Hauri, 1996; Lassiter & Hauri, 1998),

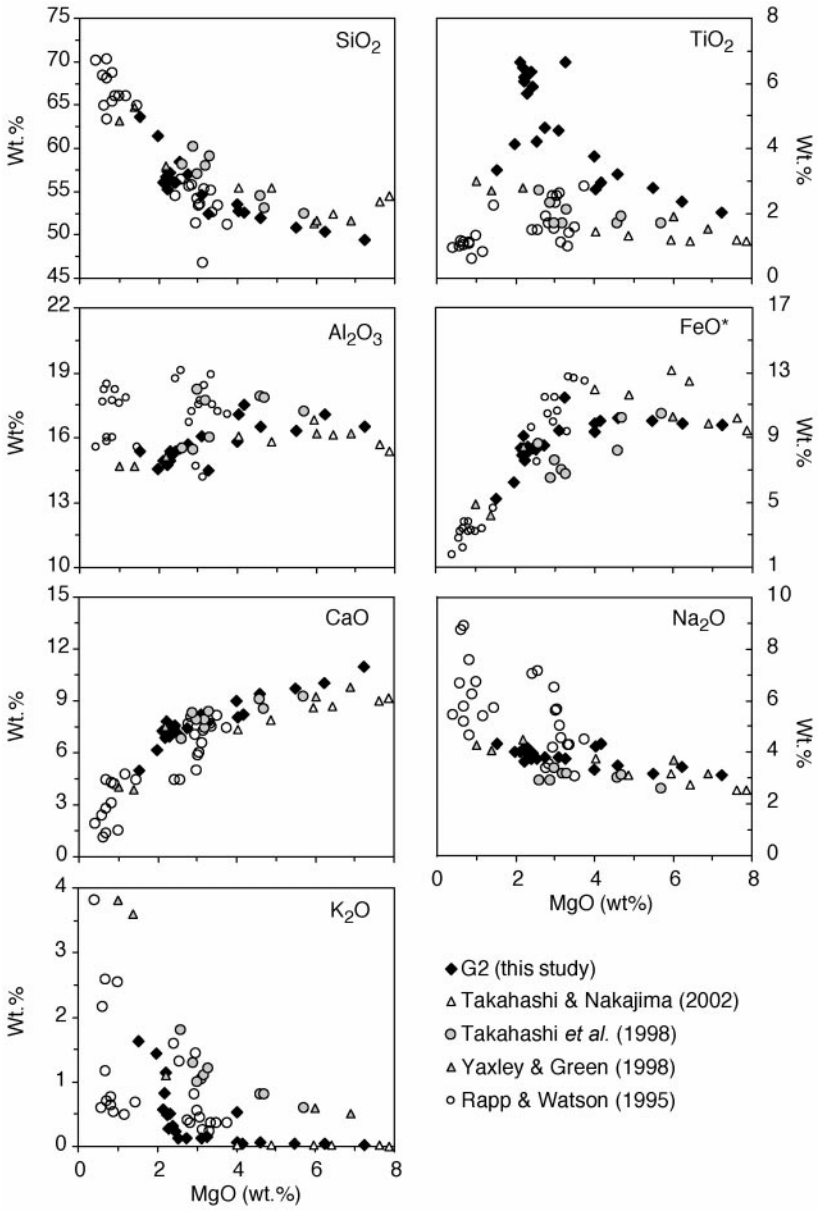

Fig. 13. Comparison of compositions of experimentally generated partial melts from hydrous and anhydrous quartz eclogite compositions between 2 and 3·5 GPa from this study (G2) and the work of Rapp & Watson (1995), Takahashi *et al.* (1998), Yaxley & Green (1998) and Takahashi & Nakajima (2002). Oxides are plotted against wt % MgO as a proxy for melt fraction instead of temperature because of the differing melting temperatures of dry and wet eclogites. Relative to anhydrous partial melts, hydrous partial melts of eclogite have lower MgO, higher SiO_2, Al_2O_3 and alkalis, and lower TiO_2 and CaO.

the Koolau lavas differ from other Hawaiian lavas in having elevated SiO_2, Na_2O/TiO_2 and Zr/Nb, and low CaO, TiO_2 and CaO/Al_2O_3 (Frey *et al.*, 1994; Hauri, 1996; Norman & Garcia, 1999; Norman *et al.*, 2002). Although most agree that these compositional characteristics are a consequence of a unique source constituent in the Koolau source, opinion is divided regarding the nature of this component. Partial melting experiments on pyroxenite compositions can aid critical examination of the hypothesis that partial melts of eclogite are the carriers of the exotic Koolau component.

One possibility is that the silica enrichment derives from addition of a high-silica (dacitic) component to otherwise normal (picritic) partial melts of the mantle (Hauri, 1996). Such dacitic liquids could originate by small-degree partial melts of hydrous or anhydrous eclogite, provided conditions (low temperature,

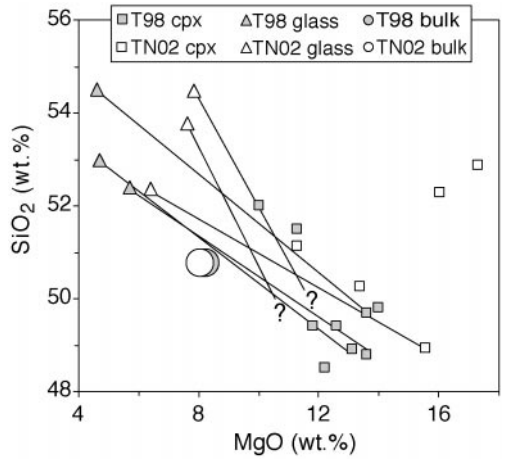

Fig. 14. Phase and bulk compositions of experiments producing high melt fractions from eclogite at 2–3 GPa from studies of Takahashi *et al.* (1998) and Takahashi & Nakajima (2002), marked as T98 and TN02, respectively. Glass compositions are shown for all experiments at 2–3 GPa that yielded only the phases cpx and glass. Also shown are bulk compositions used in experiments and the reported cpx for all experiments. In cases where coexisting cpx and glass compositions are reported, linear combinations of coexisting glass and cpx apparently are enriched in SiO_2 relative to the bulk composition. Coexisting cpx compositions are not reported for two glasses, but these experiments also apparently have mass-balance problems, provided that the glasses coexisted with realistic cpx compositions (such as those indicated by '?' symbols). A plausible explanation for these discrepancies is that the reported SiO_2 values of experimental glasses are too high.

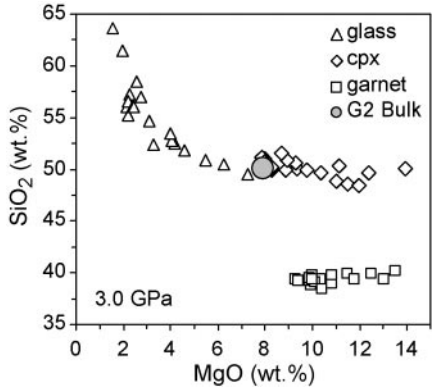

Fig. 15. Composition of coexisting garnet, cpx and glass from G2 partial melting experiments, compared with the G2 bulk composition. The SiO_2 concentrations of cpx are similar to that of the bulk composition, so SiO_2-rich liquids can form only when they are mass-balanced by an appreciable (but nevertheless small) proportion of silica-poor garnet.

relatively high availability of alkalis; see above) are appropriate for generation of high-silica, low-TiO_2 partial melts. In Fig. 16, we show an illustrative model that demonstrates the effect of such a component on parental magmas in Hawaii. As given in Table 6, we assume that the 'generic' Hawaiian parental magma is similar to Kilauea picrite KIL-1-7 (Norman & Garcia, 1999) and we assume a dacitic liquid composition consistent with the trend for anhydrous experimental partial melts illustrated in Figs 13 and 16. We presume that mixing takes place between liquid partial melts (Martin *et al.*, 1994; Class & Goldstein, 1997; Lassiter *et al.*, 2000; Reiners, 2002), meaning that the requisite proportion of eclogite in the source is much less than the proportion of dacitic melt (Hirschmann & Stolper, 1996; Pertermann & Hirschmann, 2003). Plausible MgO-rich liquids similar to primitive compositions inferred from Koolau melt inclusions (Norman *et al.*, 2002) can be generated by admixture of 10–25% dacitic and 75–90% Kilauea picritic partial melts (Fig. 16). Because of the differing expected degrees of melting of the respective source lithologies, this may correspond to perhaps 5–10% eclogite in the Koolau source. Matches are particularly good for SiO_2, CaO and CaO/Al_2O_3, but less so for TiO_2 and Na_2O/TiO_2.

It should be noted that both the dacitic component employed in the calculation in Fig. 16 and the experimentally generated dacitic partial melts of eclogite are unlike the composition inferred for the Koolau component by Hauri (1996). In particular, the latter has much higher MgO and Mg number and lower CaO and TiO_2 (Fig. 16). Perhaps elevated MgO and Mg number in a silicic magma could be a consequence of reaction with peridotite (e.g. Kelemen *et al.*, 1995), although it is not clear whether siliceous or radiogenic osmium signatures derived from partial melting of eclogite can survive high-pressure equilibration with peridotite (Hauri, 1997; Yaxley & Green, 1998).

Despite some notable successes, there are a number of problems with the idea that the Koolau component derives from a dacitic partial melt of eclogite. First, it requires mixing of small-degree partial melts of eclogite with products of partial fusion of peridotite. Yet, as also pointed out by Takahashi & Nakajima (2002), temperatures sufficient to initiate partial melting of peridotite would generate very high degrees of eclogite partial melting (Yaxley & Green, 1998; Pertermann & Hirschmann, 2003), and such large-degree partial melts are clearly not dacitic (Figs 5 and 13). Therefore, one might suppose that dacitic partial melts could form from eclogite in the deeper portions or the cold periphery of the plume, with peridotite partial melting predominantly in the hot core. Second, the Koolau component does not appear to have a strong garnet signature, as would be expected for dacitic partial melts of eclogite. For example, Sr/Y and Sm/Yb are not appreciably greater than those observed at other Hawaiian volcanoes (Norman & Garcia, 1999; Putirka, 1999). On the other hand, the high Zr/Nb in the Koolau lavas would be best explained by rutile in

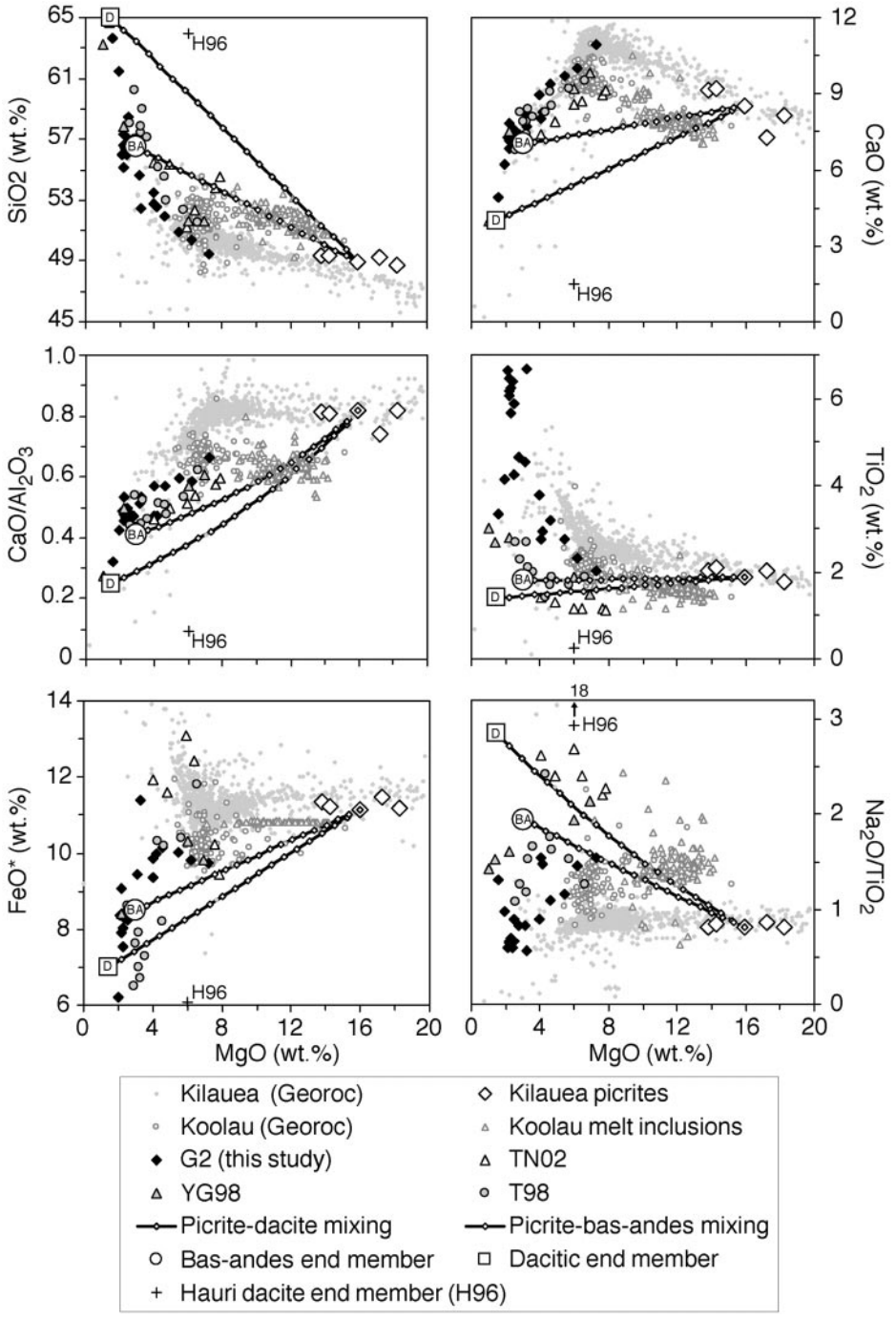

Fig. 16. Koolau magmas, represented by erupted lavas from the Georoc database (available at http://georoc.mpch-mainz.gwdg.de/) and compositions of primitive liquids reconstructed from melt inclusions (Norman *et al*., 2002), have systematically higher SiO_2 and Na_2O/TiO_2 and lower CaO, CaO/Al_2O_3, TiO_2 and FeO* than typical Hawaiian magmas, here represented by Kilauea lavas from the Georoc database and Kilauea picrites (Norman & Garcia, 1999). It should be noted that constant FeO* of compositions derived from Koolauan melt inclusions is an artifact of the technique used by Norman *et al*. (2002). Partial melts of eclogite, represented by experiments from Takahashi *et al*. (1998) (T98), Yaxley & Green (1998) (YG98), Takahashi & Nakajima (2002) (TN02) and this study have compositional features (high SiO_2 and Na_2O/TiO_2, low CaO, CaO/Al_2O_3, TiO_2 and FeO*) similar to those observed at Koolau, but markedly lower MgO than putative Koolauan parental lavas derived from melt inclusions (Norman *et al*., 2002). The figure shows calculated mixing trends between a 'normal' Hawaiian component [represented by Kilauea picrite KIL-1-7 from Norman & Garcia (1999)] with dacitic and basaltic andesitic compositions similar to the trend defined by partial melts of eclogite. Ornaments on mixing lines indicate increments of 5%, and on most trends the Koolau picrites are matched with 10–20% dacite component or 20–35% basaltic andesitic component. It should be noted that the dacitic end-member suggested by Hauri (1996) is much richer in MgO than experimentally produced dacitic partial melts of eclogite.

Table 6: Composition of potential end-members of the Koolau source

	Mixing calculations in Fig. 16			Hauri (1996)
	picrite end-member[1]	basaltic andesite[2]	dacite[2]	dacite[3]
SiO_2	48·96	56·5	65	64
TiO_2	1·89	1·8	1·4	0·25
Al_2O_3	10·45	17	16	16·35
FeO	11·14	8·5	7	6
MgO	15·97	3	1·5	6
CaO	8·53	7	4	1·5
Na_2O	1·52	3·5	4	4·5
K_2O	0·34	0·5	1	1·4
Sum	98·8	97·8	99·9	100
CaO/Al_2O_3	0·82	0·41	0·25	0·09
Na_2O/TiO_2	0·80	1·94	2·86	18·0

[1]Kilauea picrite KIL-1-7 (Norman & Garcia, 1999) assumed to be 'normal' Hawaiian end-member in Koolau source for mixing calculations shown in Fig. 16.
[2]Basaltic andesite and dacite compositions, assumed to be 'exotic' end-members in Koolau source for mixing calculations in Fig. 16.
[3]Dacite composition of exotic Koolau end-member proposed by Hauri (1996).

the source, and, as suggested above in this discussion, this is likely only at low melt fraction.

A second possibility is that silica-enriched Koolau lavas are derived directly from an intermediate silica (basaltic andesite) liquid generated by high degrees of melting of an eclogite source (Takahashi & Nakajima, 2002). In contrast to a low-degree dacitic partial melt, a high-degree basaltic andesitic melt could be generated under conditions consistent with partial melting of neighboring peridotite domains and would not have a strong garnet signature. Takahashi & Nakajima (2002) asserted that such a melt may be similar to Koolau lavas, and suggested that the latter may derive almost entirely from high-degree partial melts of eclogite. However, the high silica contents of high-degree partial melts reported by Takahashi & Nakajima (2002) may not be accurate (Fig. 14). Moreover, derivation of these lavas from basaltic andesitic partial melts of eclogite is at odds with inferences of picritic parental melts at Koolau (Norman & Garcia, 1999; Norman *et al.*, 2002).

A third possibility is that a high-MgO Koolau component could be derived by mixing of a picritic liquid, similar to that erupted at other Hawaiian volcanoes, with a basaltic andesitic liquid derived by intermediate degrees of melting of an eclogitic source. This scenario is illustrated in Fig. 16, which shows that modest proportions (20–35%) of a liquid with 56·5% silica added to Kilauean picrite KIL-1-7 (Table 6) can potentially generate a magnesian liquid similar to those reconstructed from Koolau melt inclusions (Norman *et al.*, 2002). It should be noted again that preferential melting would produce this proportion of basaltic andesitic liquid from a source with a much lower proportion of eclogitic lithology.

This third scenario yields mixed liquids that are plausible parents to Koolau lavas using an enriched end-member that is consistent with the compositional trend observed for partial melting of eclogite (Fig. 16). However, it is important to note that the basaltic andesitic composition assumed in the calculation is not that of any particular experimental glass. Partial melts of G2 and G2K bulk compositions with >55 wt % SiO_2 have been observed only at relatively low temperature at 3 GPa (Fig. 5), and so would suffer from the same objections as those outlined for dacitic partial melts above. It may be that this is owing to the relatively high TiO_2 of these bulk compositions. Higher-degree partial melts reported in the studies of Takahashi *et al.* (1998) and Takahashi & Nakajima (2002) are more similar to the hypothetical composition employed in Fig. 16. Thus, although our discussion illustrates that a basaltic andesitic component could account for many of the major element features of the Koolau component without imparting a strong garnet signature, it is unclear whether such compositions can be generated under plausible conditions. It is also not established whether the observed isotopic systematics (Hauri, 1996) can be explained in this way. For these reasons, we regard the origin of the exotic Koolau component to be unresolved.

Recycled oceanic crust in LIP sources

One of the enduring puzzles of LIPs is that they are produced at exceedingly high eruption rates. Very hot plumes could explain the high eruption rates (Farnetani & Richards, 1994), but such plumes would be expected to produce highly magnesian lavas, which are rather rare in LIPs (Cordery *et al.*, 1997). In recent years, a number of workers have proposed that large magma fluxes can be produced from eclogite-bearing plumes, without high potential temperatures (Cordery *et al.*, 1997; Takahashi *et al.*, 1998; Yasuda & Fujii, 1998; Leitch & Davies, 2001). Partial melts of eclogite may also be responsible for the unexpectedly silica-enriched compositions of the CRB (Takahashi *et al.*, 1998).

Eclogite is denser than peridotite in the upper mantle, and so may contribute negative buoyancy to

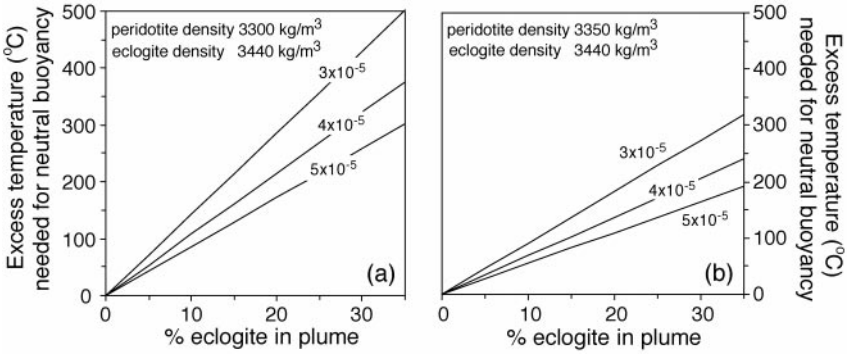

Fig. 17. Calculated minimum difference between plume temperature and that of the surrounding mantle required to generate positive plume buoyancy for a given proportion of dense eclogite contained in the plume. The calculation is based on equation (8) of Leitch & Davies (2001), with assumed eclogite density of 3440 kg/m^3 (see text), and peridotite densities of (a) 3300 kg/m^3 and (b) 3350 kg/m^3, using coefficients of thermal expansion of 3 ×, 4 × and 5 × 10^{-5}/°C.

plumes and therefore inhibit upwelling. This will limit the proportion of eclogite that can be delivered to the shallow mantle in plumes with modest temperature excess. Takahashi *et al*. (1998) argued that the CRB could result from partial melting of eclogite in a plume with a potential temperature not greatly in excess of the MORB adiabat. Takahashi & Nakajima (2002) suggested that the Koolau component in Hawaii can be produced from large eclogite blocks carried in a plume with an excess potential temperature of about 100°C. The viability of these models depends on density contrasts between eclogite and ambient mantle (e.g. Yasuda & Fujii, 1998). Eclogite is commonly assumed to have a density of 3500 kg/m^3 (Cordery *et al*., 1997; Leitch & Davies, 2001), but the low garnet mode documented in our experiments suggests that this may be too high.

We estimate the (1 atm) density of the 3 GPa subsolidus (run 166, 1300°C) assemblage using the observed modes of cpx, garnet, quartz and rutile (Tables 3–5; see also Pertermann & Hirschmannn, 2003) and densities for garnet and cpx estimated from measured compositions (Tables 4 and 5). Using the model of Geiger (2000), we calculate a density of 3880 kg/m^3 for the sub-solidus garnet in run 166. A density of 3400 kg/m^3 is estimated for the corresponding cpx, based on the volumetric parameters of Sack & Ghiorso (1994) plus the molar volume of Ca-Eskola given by McCormick (1986). This method predicts densities of CaEs-rich eclogitic cpx determined by McCormick with an average error of 0·05%. The resulting density of G2 eclogite just below its solidus is 3440 kg/m^3. This is 2·7–4·2% more dense than garnet peridotite (3300–3350 kg/m^3) and substantially less than the 4·5–6·1% contrast that is commonly assumed.

The potential temperature required to generate positive buoyancy in an eclogite-laden plume rises linearly with increase in the proportion of eclogite (Fig. 17). Depending on the assumed values of peridotite density and coefficient of thermal expansion (α), an upper-mantle plume with 10% eclogite must be 50–140°C hotter than surrounding mantle to have neutral buoyancy. One with 20% eclogite must be 110–290°C hotter. The smaller excess temperatures in these calculations correspond to denser, more fertile peridotite (3350 kg/m^3)and larger values of α (Fig. 17b). Although we do not account for the effects of depth on eclogite and garnet peridotite densities, these calculations should provide reasonable constraints in the upper mantle. Values near (2–3) × 10^{-5} are sometimes assumed for α in geophysical calculations, but the subMELTS algorithm (Asimow & Ghiorso, 1998) indicates that α of peridotite in the upper mantle is probably closer to 5 × 10^{-5}. Consequently, for a given proportion of eclogite, the smaller calculated values of excess temperature in Fig. 17 are likely to be more realistic. For this reason, and because eclogite is less dense than commonly assumed, the excess temperature required for a plume to support a given proportion of eclogite may be markedly less than previously assumed (Yasuda & Fujii, 1998; Leitch & Davies, 2001).

One of the distinctive features of the CRB is their relative enrichment in SiO_2 (Takahashi *et al*., 1998). The most voluminous portions of the CRB have 52–56% SiO_2, which Takahashi *et al*. (1998) argued could result from partial melting of abundant recycled oceanic crust in the head of the Yellowstone plume. This model may not apply to formation of other LIPs, as similar silica enrichments are not common in basalts from LIPs elsewhere. The silica enrichments in the CRB are not accompanied by a strong garnet signature and Takahashi *et al*. (1998) called on formation of 52–56 wt % SiO_2 liquids from intermediate (30–50%) extents of partial melting of a basaltic source at a pressure near 2 GPa, without significant

garnet in the residue. As with the case of Koolau, the viability of this model rests on whether appropriate silica enrichments can be generated at modest melt fractions.

ACKNOWLEDGEMENTS

H.-G. Stosch kindly provided the sample of eclogite W6.8. We thank A. D. Johnston, M. O'Hara and G. Yaxley for their supportive reviews. D. Xirouchakis and J. Simpson are thanked for help in the piston-cylinder laboratory. M.P. acknowledges funding from a University of Minnesota graduate school fellowship and the V. R. Murthy and J. Noruk fellowship of the Department of Geology and Geophysics at the University of Minnesota. This research is supported by NSF grants OCE9706526 and OCE9876255 and a University of Minnesota grant-in-aid to M.M.H.

REFERENCES

Asimow, P. D. & Ghiorso, M. S. (1998). Algorithmic modifications extending MELTS to calculate subsolidus phase relations. *American Mineralogist* **83**, 1127–1132.

Baker, M. B. & Stolper, E. M. (1994). Determining the composition of high-pressure mantle melts using diamond aggregates. *Geochimica et Cosmochimica Acta* **58**, 2811–2827.

Baker, M. B., Hirschmann, M. M., Wasylenki, L. E., Stolper, E. M. & Ghiorso, M. S. (1996). Quest for low-degree mantle melts—reply. *Nature* **381**, 286.

Barth, M. G., Rudnick, R. L., Horn, I., McDonough, W. F., Spicuzza, M. J., Valley, J. W. & Haggerty, S. E. (2001). Geochemistry of xenolithic eclogites from West Africa, Part I: A link between low MgO eclogites and Archaean crust formation. *Geochimica et Cosmochimica Acta* **65**, 1499–1527.

Basaltic Volcanism Study Project (1981). *Basaltic Volcanism on the Terrestrial Planets*. New York: Pergamon.

Becker, H. (2000). Re–Os fractionation in eclogites and blueschists and the implications for recycling of oceanic crust into the mantle. *Earth and Planetary Science Letters* **177**, 287–300.

Blundy, J. D., Falloon, T. J., Wood, B. J. & Dalton, J. A. (1995). Sodium partitioning between clinopyroxene and silicate melts. *Journal of Geophysical Research* **100**, 15501–15516.

Chase, C. G. (1981). Oceanic island Pb: two-stage histories and mantle evolution. *Earth and Planetary Science Letters* **52**, 277–284.

Chase, C. G. & Patchett, P. J. (1988). Stored mafic/ultramafic crust and early Archaean mantle depletion. *Earth and Planetary Science Letters* **91**, 66–72.

Class, C. & Goldstein, S. L. (1997). Plume–lithosphere interactions in the ocean basins: constraints from the source mineralogy. *Earth and Planetary Science Letters* **150**, 245–260.

Cordery, M. J., Davies, G. F. & Campbell, I. H. (1997). Genesis of flood basalts from eclogite-bearing mantle plumes. *Journal of Geophysical Research* **102**, 20179–20197.

Dickey, J. S. (1970). Partial fusion products in alpine-type peridotites; Serrania de la Ronda and other examples. *Special Paper—Mineralogical Society of America* **3**, 33–49.

Eiler, J. M., Schiano, P., Kitchen, N. & Stolper, E. M. (2000). Oxygen-isotope evidence for recycled crust in the sources of mid-ocean-ridge basalts. *Nature* **403**, 530–534.

Ellis, D. J. & Green, D. H. (1979). An experimental study of the effect of Ca upon the garnet–clinopyroxene Fe–Mg exchange equilibria. *Contributions to Mineralogy and Petrology* **71**, 13–22.

Falloon, T. J., Green, D. H., O'Neill, H. S. C. & Ballhaus, C. G. (1996). Quest for low-degree mantle melts. *Nature* **381**, 285.

Falloon, T. J., Green, D. H., Danyushevsky, L. V. & Faul, U. H. (1999). Peridotite melting at 1·0 and 1·5 GPa: an experimental evaluation of techniques using diamond aggregates and mineral mixes for determination of near-solidus metals. *Journal of Petrology* **40**, 1343–1375.

Farnetani, C. G. & Richards, M. A. (1994). Numerical investigations of the mantle plume initiation model for flood basalt events. *Journal of Geophysical Research* **99**, 13818–13833.

Foley, S. F., Barth, M. G. & Jenner, G. A. (2000). Rutile/melt partition coefficients for trace elements and an assessment of the influence of rutile on the trace element characteristics of subduction zone magmas. *Geochimica et Cosmochimica Acta* **64**, 933–938.

Frey, F. A., Garcia, M. O. & Roden, M. F. (1994). Geochemical characteristics of Koolau Volcano; implications of intershield geochemical differences among Hawaiian volcanoes. *Geochimica et Cosmochimica Acta* **58**, 1441–1462.

Gaetani, G. A., Asimow, P. D. & Stolper, E. M. (1998). Determination of the partial molar volume of SiO_2 in silicate liquids at elevated pressures and temperatures; a new experimental approach. *Geochimica et Cosmochimica Acta* **62**, 2499–2508.

Geiger, C. A. (2000). Volumes of mixing in aluminosilicate garnets: solid solution and strain behavior. *American Mineralogist* **85**, 893–897.

Green, T. H., Blundy, J. D., Adam, J. & Yaxley, G. M. (2000). SIMS determination of trace element partition coefficients between garnet, clinopyroxene and hydrous basaltic liquids at 2–7·5 GPa and 1080–1200 degrees C. *Lithos* **53**, 165–187.

Hauri, E. H. (1996). Major-elements variability in the Hawaiian mantle plume. *Nature* **382**, 415–419.

Hauri, E. H. (1997). Melt migration and mantle chromatography; 1, Simplified theory and conditions for chemical and isotopic decoupling. *Earth and Planetary Science Letters* **153**, 1–19.

Helffrich, G. R. & Wood, B. J. (2001). The Earth's mantle. *Nature* **412**, 501–507.

Hemingway, B. S., Bohlen, S. R., Hankins, W. B., Westrum, E. F., Jr & Kuskov, O. L. (1998). Heat capacity and thermodynamic properties for coesite and jadeite, reexamination of the quartz–coesite equilibrium boundary. *American Mineralogist* **83**, 409–418.

Hess, P. C. (1995). Thermodynamic mixing properties and the structure of silicate melts. In: Stebbins, J. F., McMillan, P. F. & Dingwell, D. M. (eds) *Structure, Dynamics and Properties of Silicate Melts. Mineralogical Society of America, Reviews in Mineralogy* **32**, 145–189.

Hirose, K. & Kushiro, I. (1993). Partial melting of dry peridotites at high pressure: determination of compositions of melts segregated from peridotites using aggregates of diamonds. *Earth and Planetary Science Letters* **114**, 477–489.

Hirschmann, M. M. (2000). Mantle solidus: experimental constraints and the effects of peridotite composition. *Geochemistry, Geophysics, Geosystems* **1**, 2000GC000070.

Hirschmann, M. M. & Stolper, E. M. (1996). A possible role for garnet pyroxenite in the origin of the 'garnet signature' in MORB. *Contributions to Mineralogy and Petrology* **124**, 185–208.

Hirschmann, M. M., Baker, M. B. & Stolper, E. M. (1998). The effect of alkalis on the silica content of mantle-derived melts. *Geochimica et Cosmochimica Acta* **62**, 883–902.

Hirschmann, M. M., Kogiso, T., Baker, M. B. & Stolper, E. M. (2003). Alkalic magmas generated by partial melting of garnet pyroxenite. *Geology* **31**, 481–484.

Hofmann, A. W. (1997). Mantle geochemistry; the message from oceanic volcanism. *Nature* **385**, 219–229.

Hofmann, A. W. & White, R. S. (1982). Mantle plumes from ancient oceanic crust. *Earth and Planetary Science Letters* **57**, 421–436.

Jacob, D., Jagoutz, E., Lowry, D., Mattey, D. & Kudrjavseva, G. (1994). Diamondiferous eclogites from Siberia; remnants of Archaean oceanic crust. *Geochimica et Cosmochimica Acta* **58**, 5191–5207.

Johnston, A. D. (1986). Anhydrous P–T phase relations of near-primary high-alumina basalt from the South Sandwich Islands. *Contributions to Mineralogy and Petrology* **92**, 368–382.

Kelemen, P. B., Shimizu, N. & Salters, V. J. M. (1995). Extraction of mid-ocean-ridge basalt from the upwelling mantle by focused flow of melt in dunite channels. *Nature* **375**, 747–753.

Kellogg, L. H. & Turcotte, D. L. (1990). Mixing and the distribution of heterogeneities in a chaotically convecting mantle. *Journal of Geophysical Research* **95**, 421–432.

Klein, M., Stosch, H.-G., Seck, H. A. & Shimizu, N. (2000). Experimental partitioning of high field strength and rare earth elements between clinopyroxene and garnet in andesitic to tonalitic systems. *Geochimica et Cosmochimica Acta* **64**, 99–115.

Klemme, S., Blundy, J. D. & Wood, B. J. (2002). Experimental constraints on major and trace element partitioning during partial melting of eclogite. *Geochimica et Cosmochimica Acta* **66**, 3109–3123.

Kogiso, T., Tatsumi, Y. & Nakano, S. (1997*a*). Trace element transport during dehydration processes in the subducted oceanic crust: 1. Experiments and implications for the origin of ocean island basalts. *Earth and Planetary Science Letters* **148**, 193–205.

Kogiso, T., Tatsumi, Y., Shimoda, G. & Barsczus, H. G. (1997*b*). High μ (HIMU) ocean island basalts in southern Polynesia: new evidence for whole mantle scale recycling of subducted oceanic crust. *Journal of Geophysical Research* **102**, 8085–8103.

Kogiso, T., Hirose, K. & Takahashi, E. (1998). Melting experiments on homogeneous mixtures of peridotite and basalt: application to the genesis of ocean island basalts. *Earth and Planetary Science Letters* **162**, 45–61.

Kogiso, T., Hirschmann, M. M. & Frost, D. J. (2003). High pressure partial melting of garnet pyroxenite: possible mafic lithologies in the source of ocean island basalts. *Earth and Planetary Science Letters* (in press).

Kornprobst, J. (1969). Le massif ultrabasique des Beni Bouchera (Rif interne, Maroc); étude des peridotites de haute température et de haute pression, et des pyroxenolites, à grenat ou sans grenat, qui leur sont associées. *Journal of Contributions to Mineralogy and Petrology* **23**, 283–322.

Kushiro, I. (1975). Nature of silicate melt and its significance in magma genesis—regularities in shift of liquidus boundaries involving olivine, pyroxene, and silica minerals. *American Journal of Science* **275**, 411–431.

Langmuir, C. H., Klein, E. M. & Plank, T. (1992). Petrological systematics of mid-ocean ridge basalts: constraints on melt generation beneath ocean ridges. In: Morgan, J. P., Blackman, D. K. & Sinton, J. M. (eds) *Mantle Flow and Melt Generation at Mid-Ocean Ridges*. *Geophysical Monograph, American Geophysical Union* **71**, 183–280.

Lassiter, J. C. & Hauri, E. H. (1998). Osmium-isotope variations in Hawaiian lavas: evidence for recycled oceanic lithosphere in the Hawaiian plume. *Earth and Planetary Science Letters* **164**, 483–496.

Lassiter, J. C., Hauri, E. H., Reiners, P. W. & Garcia, M. O. (2000). Generation of Hawaiian post-erosional lavas by melting of a mixed lherzolite/pyroxenite source. *Earth and Planetary Science Letters* **178**, 269–284.

Leitch, A. M. & Davies, G. F. (2001). Mantle plumes and flood basalts: enhanced melting from plume ascent and an eclogite component. *Journal of Geophysical Research* **106**, 2047–2059.

Longhi, J. (2002). Some phase equilibrium systematics of lherzolite melting: I. *Geochemistry, Geophysics, Geosystems* **3**, 2001GC000204.

Loubet, M. & Allègre, C. J. (1982). Trace elements in orogenic lherzolites reveal the complex history of the upper mantle. *Nature* **298**, 809–814.

Lundstrom, C. C., Gill, J., Williams, Q. & Perfit, M. (1995). Mantle melting and basalt extraction by equilibrium porous flow. *Science* **270**, 1958–1961.

Martin, C. E., Carlson, R. W., Shirey, S. B., Frey, F. A. & Chen, C.-Y. (1994). Os isotopic variation in basalts from Haleakala Volcano, Maui, Hawaii; a record of magmatic processes in oceanic mantle and crust. *Earth and Planetary Science Letters* **128**, 287–301.

McCormick, T. C. (1986). Crystal-chemical aspects of non-stoichiometric pyroxenes. *American Mineralogist* **71**, 1434–1440.

Morgan, G. B. & London, D. (1996). Optimizing the electron microprobe analysis of hydrous alkali aluminosilicate glasses. *American Mineralogist* **81**, 1176–1185.

Morgan, J. P. & Morgan, W. J. (1999). Two-stage melting and the geochemical evolution of the mantle: a recipe for mantle plum-pudding. *Earth and Planetary Science Letters* **170**, 215–239.

Norman, M. D. & Garcia, M. O. (1999). Primitive magmas and source characteristics of the Hawaiian plume: petrology and geochemistry of shield picrites. *Earth and Planetary Science Letters* **168**, 27–44.

Norman, M. D., Garcia, M. O., Kamenetsky, V. S. & Nielsen, R. L. (2002). Olivine-hosted melt inclusions in Hawaiian picrites: equilibration, melting, and plume source characteristics. *Chemical Geology* **183**, 143–168.

Nicolas, A., Bouchez, J. L. & Boudier, F. (1972). Interprétation cinématique des déformations plastiques dans le Massif de lherzolite de Lanzo (Alpes piemontaises); comparaison avec d'autres massifs. *Tectonophysics* **14**, 143–171.

Niu, Y. L. & Batiza, R. (1997). Trace element evidence from seamounts for recycled oceanic crust in the Eastern Pacific mantle. *Earth and Planetary Science Letters* **148**, 471–483.

Pertermann, M. & Hirschmann, M. M. (2002). Trace-element partitioning between vacancy-rich eclogitic clinopyroxene and silicate melt. *American Mineralogist* **87**, 1365–1376.

Pertermann, M. & Hirschmann, M. M. (2003). Partial melting experiments on a MORB-like pyroxenite between 2 and 3 GPa: constraints on the presence of pyroxenites in basalt source regions. *Journal of Geophysical Research* **108**(B2), 10.1029/2000JB000118.

Pickering-Witter, J. M. & Johnston, A. D. (2000). The effects of variable mineral proportions on the melting systematics of fertile peridotite assemblages. *Contributions to Mineralogy and Petrology* **140**, 190–211.

Putirka, K. (1999). Clinopyroxene + liquid equilibria to 100 kbar and 2450 K. *Contributions to Mineralogy and Petrology* **135**, 151–163.

Rapp, R. P. and Watson, E. B. (1995). Dehydration melting of metabasalt at 8–32 kbar; implications for continental growth and crust–mantle recycling. *Journal of Petrology* **36**, 891–931.

Ravna, E. K. (2000). The garnet–clinopyroxene Fe^{2+}–Mg geothermometer: an updated calibration. *Journal of Metamorphic Geology* **18**, 211–219.

Reiners, P. W. (2002). Temporal–compositional trends in intraplate basalt eruptions: implications for mantle heterogeneity and melting processes. *Geochemistry, Geophysics, Geosystems* **3**, 2001GC000250.

Robinson, J. A. C., Wood, B. J. & Blundy, J. D. (1998). The beginning of melting of fertile and depleted peridotite at 1·5 GPa. *Earth and Planetary Science Letters* **155**, 97–111.

Rudnick, R. L., Barth, M., Horn, I. & McDonough, W. F. (2000). Rutile-bearing refractory eclogites; missing link between continents and depleted mantle. *Science* **287**, 278–281.

Ryerson, F. J. (1985). Oxide solution mechanisms in silicate melts; systematic variations in the activity coefficient of SiO_2. *Geochimica et Cosmochimica Acta* **49**, 637–649.

Ryerson, F. J. & Watson, E. B. (1987). Rutile saturation in magmas; implications for Ti–Nb–Ta depletion in island-arc basalts. *Earth and Planetary Science Letters* **86**, 225–239.

Sack, R. O. & Ghiorso, M. S. (1994). Thermodynamics of multicomponent pyroxenes; I, Formulation of a general model. *Contributions to Mineralogy and Petrology* **116**, 277–286.

Schulze, D. J., Valley, J. W. & Spicuzza, M. J. (2000). Coesite eclogites from the Roberts Victor Kimberlite, South Africa. *Lithos* **54**, 23–32.

Schwab, B. E. & Johnston, A. D. (2001). Melting systematics of modally variable, compositionally intermediate peridotites and the effects of mineral fertility. *Journal of Petrology* **42**, 1789–1811.

Smyth, J. R. (1980). Cation vacancies and the crystal chemistry of breakdown reactions in kimberlitic omphacites. *American Mineralogist* **65**, 1185–1191.

Stosch, H.-G. & Lugmair, G. W. (1990). Geochemistry and evolution of MORB-type eclogites from the Münchberg Massif, southern Germany. *Earth and Planetary Science Letters* **99**, 230–249.

Stracke, A., Salters, V. J. M. & Sims, K. W. W. (1999). Assessing the presence of garnet-pyroxenite in the mantle sources of basalts through combined hafnium–neodymium–thorium isotope systematics. *Geochemistry, Geophysics, Geosystems* **1**, 1999GC000013.

Sykes, D. & Kubicki, J. D. (1994) A model for H_2O solubility mechanisms in albite melts from infrared-spectroscopy and molecular-orbital calculations. *Geochimica et Cosmochimica Acta* **57**, 1039–1052.

Takahashi, E. & Nakajima, K. (2002). Melting process in the Hawaiian plume: an experimental study. In: Takahashi, E., Lipman, P. W., Garcia, M. O., Naka, J. & Aramake, S. (eds) *Hawaiian Volcanoes: Deep Underwater Perspectives. Geophysical Monograph, American Geophysical Union* **128**, 403–418.

Takahashi, E., Nakajima, K. & Wright, T. L. (1998). Origin of the Columbia River basalts: melting model of a heterogeneous plume head. *Earth and Planetary Science Letters* **162**, 63–80.

Taylor, W. R. & Green, D. H. (1989). The role of reduced CNO–H fluid in mantle partial melts. In: *Kimberlites and Related Rocks: Proceedings of the 4th International Kimberlite Conference, Vol. 1.* Oxford: Blackwell Scientific, pp. 592–602.

Ulmer, P. & Luth, R. W. (1991). The graphite–COH fluid equilibrium in P, T, fO_2 space: an experimental determination to 30 kbar and 1600°C. *Contributions to Mineralogy and Petrology* **106**, 265–272.

van Keken, P. E., Hauri, E. H. & Ballentine, C. J. (2002). Mantle mixing: the generation, preservation, and destruction of chemical heterogeneity. *Annual Review of Earth and Planetary Sciences* **30**, 493–525.

Walter, M. J. (1998). Melting of garnet peridotite and the origin of komatiite and depleted lithosphere. *Journal of Petrology* **39**, 29–60.

Walter, M. J., Sisson, T. W. & Presnall, D. C. (1995). A mass proportion method for calculating melting reactions and application to melting of model upper mantle lherzolite. *Earth and Planetary Science Letters* **135**, 77–90.

Wasylenki, L. E., Baker, M. B., Kent, A. J. R. & Stolper, E. M. (2003). Near-solidus melting of the shallow upper mantle: partial melting experiments on depleted peridotite. *Journal of Petrology* **44**, 1163–1191.

Weaver, B. L. (1991). The origin of ocean island basalt end-member compositions: trace element and isotopic constraints. *Earth and Planetary Science Letters* **104**, 381–397.

Wright, T. L., Mangan, M. & Swanson, D. A. (1988). Chemical data for flows and feeder dikes of the Yakima basalt group, Columbia River basalt group, Washington, Oregon, and Idaho, and their bearing on a petrogenetic model. *US Geological Survey Bulletin* **1821**, 71 pp.

Xirouchakis, D., Hirschmann, M. M. & Simpson, J. A. (2001). The effect of titanium on the silica content and on mineral–liquid partitioning of mantle-equilibrated melts. *Geochimica et Cosmochimica Acta* **65**, 2201–2217.

Yasuda, A. & Fujii, T. (1998). Ascending subducted oceanic crust entrained within mantle plumes. *Geophysical Research Letters* **25**, 1561–1564.

Yasuda, A., Fujii, T. & Kurita, K. (1994). Melting phase relations of an anhydrous mid-ocean ridge basalt from 3 to 20 GPa; implications for the behavior of subducted oceanic crust in the mantle. *Journal of Geophysical Research* **99**, 9401–9414.

Yaxley, G. M. & Green, D. H. (1998). Reactions between eclogite and peridotite: mantle refertilization by subduction of oceanic crust. *Schweizerische Mineralogische und Petrographische Mitteilungen* **78**, 243–255.

Zindler, A. & Hart, S. (1986). Chemical geodynamics. *Annual Review of Earth and Planetary Sciences* **14**, 493–571.

Zindler, A., Staudigel, H. & Batiza, R. (1984). Isotope and trace element geochemistry of young Pacific seamounts: implications for the scale of upper mantle heterogeneity. *Earth and Planetary Science Letters* **70**, 175–195.